

The nature of faint submillimetre-selected galaxies

Ian Smail,¹ R. J. Ivison,^{2,3} A. W. Blain^{4,5} & J.-P. Kneib⁶

¹ *Department of Physics, University of Durham, South Road, Durham DH1 3LE*

² *Astronomy Technology Centre, Royal Observatory, Blackford Hill, Edinburgh EH9 3HJ*

³ *Department of Physics & Astronomy, University College London, Gower Street, London WC1E 6BT*

⁴ *Department of Astronomy, Caltech, Pasadena, CA 91125, USA*

⁵ *Institute of Astronomy, Madingley Road, Cambridge CB3 0HA*

⁶ *Observatoire de Toulouse, 14 avenue E. Belin, 31400 Toulouse, France*

Accepted 2001 November 29. Received 2001 April 27; in original form 2001 January 22

ABSTRACT

We present the source catalogue for the SCUBA Lens Survey. We summarise the results of extensive multi-wavelength observations of the 15 submillimetre-selected galaxies in the catalogue, from X-rays to radio. We discuss the main observational characteristics of faint submillimetre galaxies as a population, and consider their interpretation within the framework of our understanding of galaxy formation and evolution.

Key words: galaxies: starburst – galaxies: evolution – galaxies: formation – cosmology: observations – cosmology: early Universe – gravitational lensing

1 INTRODUCTION

The highly successful far-infrared (IR) all-sky survey undertaken by *IRAS* led to the identification of numerous highly obscured star-forming and active galaxies in the local Universe, $z \lesssim 0.3$ (Soifer, Neugebauer & Houck 1987). These systems are some of the most luminous galaxies at the present day and emit most of their radiation in the far-IR waveband, although they contribute only 0.3 per cent of the local luminosity density (Sanders & Mirabel 1996).

More recent work in the far-IR and submillimetre (submm) wavebands has produced a similar revolution in our view of obscured galaxies in the *distant* $z \gtrsim 1$ Universe. These observations have employed the *COBE* and *ISO* satellites and the Submm Common-User Bolometer Array (SCUBA; Holland et al. 1999) on the 15-m James Clerk Maxwell Telescope* (JCMT). The new observations have shown that the ultraluminous far-IR population evolves more strongly than the equivalent optically-selected population and that, in contrast to the local Universe, luminous obscured galaxies at high redshift could contribute a substantial fraction of the total emitted radiation.

This conclusion is confirmed by comparing the energy density in the optical (Bernstein et al. 2001) and far-IR/submm backgrounds (Puget et al. 1996; Fixsen et al. 1998; Finkbeiner, Schlegel & Davis 2000). These backgrounds represent the cumulative energy emitted in these

wavebands across all epochs, mainly at redshift $z \sim 1$. The approximate equivalence of the energy density in the two regimes shows that somewhere near half of the total radiation in the Universe came from obscured energy sources, which could be either stars or AGN. If the majority of this emission is powered by radiation from stars with a standard initial mass function (IMF), then approximately half of all the stars that have formed by the present day could have formed in highly obscured systems. Clearly it is critically important to include these highly-obscured sources in models of galaxy evolution if we are to obtain a complete understanding of the formation and evolution of galaxies.

The advent of sensitive submm imaging with SCUBA has allowed a number of groups to undertake surveys for distant submm galaxies. Results on the number density of sources in blank fields as a function of 850- μm flux density have been published by three groups: Hughes et al. (1998) worked with a single deep map centred on the *Hubble Deep Field* (HDF), while Barger et al. (1998, 1999b) employed a combination of deep/narrow and wide/shallow observations of fields in the Lockman Hole and Hawaii Survey Field regions; finally, there has been a survey of areas from the Canada-France Redshift Survey (Eales et al. 1999, 2000; Lilly et al. 1999). Shallower, wider surveys have also been carried out by Borys et al. (2001) and by the UK Submm Survey consortium (Dunlop 2001; Scott et al. 2001; Fox et al. 2001; Almaini et al. 2001). Due to the modest resolution of SCUBA, 15'' FWHM at 850 μm , the deepest of these studies are confusion limited at ~ 2 mJy (Hughes et al. 1998); this is the deepest flux density for which reliable source detection is possible in blank fields (Blain, Ivison & Smail 1998; Hogg 2001).

* The JCMT is operated by the Joint Astronomy Centre on behalf of the United Kingdom Particle Physics and Astronomy Research Council (PPARC), the Netherlands Organisation for Scientific Research, and the National Research Council of Canada.

At slightly longer wavelengths, observations using the MAMBO 1.2-mm camera on the IRAM 30-m telescope have recently been reported in both field and lensing cluster regions (Bertoldi et al. 2000).

Rather than mapping large fields, another approach to construct large samples of submm-detected galaxies is to exploit the tight correlation between the far-infrared and radio luminosities of star-forming galaxies (Condon 1992) and use SCUBA to target samples of faint radio sources (Chapman et al. 2001b, 2001c). This innovative technique is particularly well-suited for identifying the wide-field samples needed to tackle issues such as the clustering strength of SCUBA galaxies (e.g. Almaini et al. 2001).

Our collaboration has adopted yet another approach with the aim of pushing below the confusion limit of the blank-field surveys. We achieve this by using massive gravitational cluster lenses to increase both the sensitivity and resolution of SCUBA (Blain 1998). The first submm counts were based on maps of two clusters (Smail, Ivison & Blain 1997). The survey was subsequently expanded to cover seven lensing clusters at $z = 0.19\text{--}0.41$ (Smail et al. 1998). The results of similar surveys have recently been reported by Chapman et al. (2001) and van der Werf et al. (2001b). These observations of lensing clusters benefit from a typical amplification factor of $2\text{--}3\times$, improving both the sensitivity of the maps and their effective resolution, and so allowing confusion-free counts to be derived down to ~ 0.5 mJy (Blain et al. 1999a), well below the conventional 2-mJy field confusion limit for SCUBA. In fortuitous cases, the amplification can exceed $10\times$ (e.g. van der Werf et al. 2001b), providing the opportunity to identify submm galaxies as faint as ~ 0.1 mJy and study their properties.

Based upon this survey we have published the number counts of submm galaxies (Smail, Ivison & Blain 1997; Blain et al. 1999a), the identification of the counterparts to the submm sources in the optical (Smail et al. 1998), near-infrared (Smail et al. 1999a; Frayer et al. 2000), radio (Smail et al. 2000) and X-ray (Fabian et al. 2000) bands, as well as optical spectroscopy of candidate counterparts (Barger et al. 1999a). We have also provided detailed multi-wavelength follow-up observations of the brighter sources (Ivison et al. 1998a, 2000a). Building on the redshifts determined for the three brightest sources in the sample, we have obtained the first CO detections of submm-selected galaxies using the OVRO and IRAM interferometers (Frayer et al. 1998, 1999; Kneib et al. 2001). Yet higher-resolution CO images of one source have been obtained by combining data from the OVRO and BIMA arrays (Ivison et al. 2001). High-resolution mm-continuum observations using the OVRO array have also been presented (Frayer et al. 2000). Similar mm-continuum observations of sources in other SCUBA surveys have been presented by Downes et al. (1999), Gear et al. (2000) and Lutz et al. (2001). Finally, the interpretation of these observations and their relevance to our understanding of galaxy formation and evolution at high redshifts has been discussed by Blain et al. (1999b, 1999c). This paper includes a summary and update of these previous results.

As a benchmark for the following discussion we note that an Ultraluminous Infrared Galaxy (ULIRG) with a far-IR luminosity of $L_{\text{FIR}} \sim 3 \times 10^{12} L_{\odot}$ (similar to Arp 220), and thus a star-formation rate (SFR) of $\sim 300 M_{\odot} \text{yr}^{-1}$ would have a $850\text{-}\mu\text{m}$ flux density of $\gtrsim 3$ mJy out to $z \sim 10$ in a Uni-

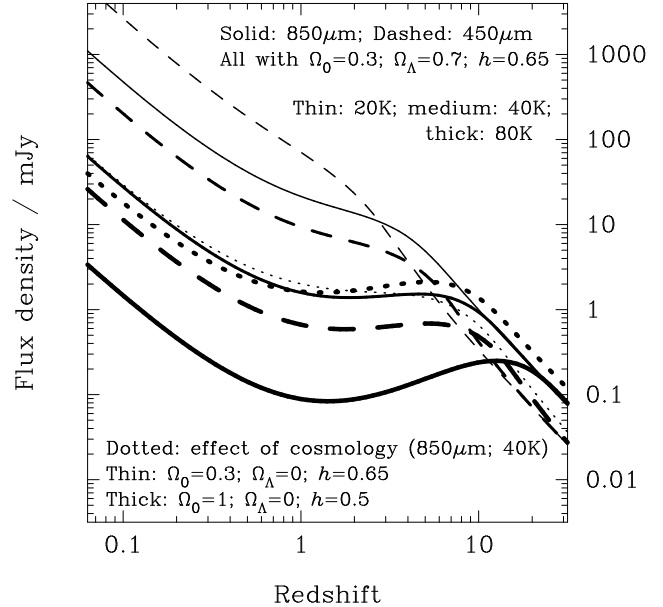


Figure 1. The flux density at 450 and 850 μm expected from a ULIRG-like galaxy as a function of redshift for different dust temperatures and cosmologies. The galaxy is assumed to have $L_{\text{FIR}} = 3 \times 10^{12} L_{\odot}$.

verse with $q_0 = 0.5$.[†] The effects of different SEDs and world models on the results in the two SCUBA observing bands are illustrated in Fig. 1. In three 8-hr shifts of observing in good conditions with SCUBA it is possible to achieve a 3σ flux limit of 3 mJy at 850 μm across a $160''$ -diameter field (upgrades to SCUBA now mean that this limit is reached in closer to two shifts), probing a volume of 10^6 Mpc^3 out to $z \sim 10$ for ULIRGs.

Here we present the source catalogue of luminous submm galaxies from our SCUBA survey, and discuss the current identifications and properties of their counterparts in other wavebands. We then summarise the broad characteristics of the populations that contribute to the submm background radiation. In §2 we briefly describe the submm observations and their reduction and analysis. In §3 we present our updated estimate of the source counts at 850 and 450 μm , and in §4 we describe the identification of counterparts and constraints on their likely redshifts and power sources. A brief summary of the characteristics of each source is given in §5, and we discuss the properties of the different classes of submm galaxy in §6. In §7 we present the main conclusions arising from the SCUBA lens survey and summarise these in §8.

2 SUBMM OBSERVATIONS, REDUCTION AND ANALYSIS

These data were obtained using SCUBA (Holland et al. 1999) on the JCMT. SCUBA contains a range of detectors and detector arrays cooled to 0.1 K covering the atmospheric

[†] We assume $q_0 = 0.5$ and $H_0 = 50 \text{ km s}^{-1} \text{ Mpc}^{-1}$ throughout the paper, except in Fig. 1.

windows from $350\ \mu\text{m}$ to $2000\ \mu\text{m}$. In our survey, we operated the 91-element short-wave array at $450\ \mu\text{m}$ and the 37-element long-wave array at $850\ \mu\text{m}$, giving half-power beam widths of $7.5''$ and $14.7''$ respectively. Operating in its conventional ‘stare’ or ‘jiggle’ mode and discarding the noisy map edges, the short- and long-wave arrays have effective fields of view of $2.3'$ and $2.8'$ respectively. The design of the optics ensures that a suitable jiggle pattern for the chopping secondary mirror can fully sample the image plane simultaneously at 450 and $850\ \mu\text{m}$. The multiplexing and high efficiency of the arrays means that SCUBA maps three orders of magnitude faster than previous submm detectors.

The clusters exploited in our survey are all well-studied, massive systems, which exhibit strongly-lensed (i.e. high-amplification) images of background galaxies (most with measured spectroscopic redshifts) that are employed to accurately model the mass distribution within the cluster (see Kneib et al. 1996; Smith et al. 2001a). These models can then be used to ‘correct’ the submm observations to derive the true fluxes of sources identified in our SCUBA maps (Blain et al. 1999a; §3). The clusters and field centres for our observations are listed in Table 1.

The submm maps of the seven clusters used in our analysis were obtained from SCUBA observations on the nights of 1997 July 02–05, 1997 August 09–14 and 21–22, 1997 September 22, 1997 December 19, 1998 January 26, 29 and 31, 1998 February 01, 1998 March 12–13 and 1998 April 03. The typical integration time was 25–35 ks and the maps have effective noise levels of $\sim 1.7\ \text{mJy rms}$ at $850\ \mu\text{m}$ (Table 1).

The observations employed a 64-point jiggle pattern, fully sampling both arrays over a period of 128 s. The pattern was subdivided into nod cycles so that the target position was switched between the signal and reference positions (separated by $60''$ in azimuth) in a repeating signal–reference–reference–signal scheme, with sixteen 1-s jiggles in each position. As well as tracing out the jiggle pattern, the secondary was chopped at $\simeq 7\ \text{Hz}$, also by $60''$ in azimuth.

A side effect of this complex procedure is the creation of two *negative* images of any source in the field, each $-1/2\times$ the intensity of the source and separated from the source in azimuth by $60''$. Since SCUBA has no image rotator, the positions of these negative sources migrate slowly around the source during each integration. Azimuthal chopping has advantages; sky removal is optimised and the field rotation means that additional real sources are less likely to be consistently nullified, however it carries a penalty: unlike nodding and chopping in R.A./Dec. coordinates (the mode now used as standard; see Ivison et al. 2000b), information contained in the negative images of each source is difficult to recover. Moreover, the noise levels we quote inevitably include a contribution from the negative images of real, bright sources as well as from faint sources below our detection threshold (i.e. conventional confusion noise).

The pointing stability was checked every hour and regular skydips were performed to measure the atmospheric opacity, which averaged 0.2 at $850\ \mu\text{m}$ and 1.0 at $450\ \mu\text{m}$, and was as good as 0.09 and 0.4 on respectively on occasion. The rms pointing errors were typically $2''$ (see §4.3).

The dedicated SCUBA data reduction software (SURF, Jenness 1997) was used to reduce the observations. The reduction consisted of subtracting the reference from the signal on a second-by-second basis, giving 1280 data points per

bolometer per 20-integration scan, where an integration represents the time needed to complete a full jiggle pattern (64 s in both the reference and signal positions). The data were flatfielded and corrected for atmospheric attenuation, then inspected statistically and visually. Some were rejected on the basis of large deviations from a bolometer’s mean, some others on the basis of noticeably peculiar behaviour. Data from bolometers suffering excessively from $1/f$ noise were also flagged as bad and removed from the analysis. At this stage, median values evaluated across the whole array were used to compensate for the spatially-correlated sky emission, reducing the effective noise-equivalent flux density to $75\text{--}90\ \text{mJy Hz}^{-1/2}$ at $850\ \mu\text{m}$ (see Ivison et al. 1998b).

The sky position appropriate for each data point is known, based on the flatfield (a file containing the relative bolometer sensitivities and positions) and the jiggle pattern, so maps can be generated by placing data from each bolometer on to an astrometric grid of $2''$ and $4''$ pixels at 450 and $850\ \mu\text{m}$ respectively (approximately Nyquist sampling). Data values more than 4σ from each pixel’s mean were rejected and pixels closer than $14''$ (one beamwidth) to the most extreme jiggle positions (regions with low effective exposure times) were blanked out from the map.

The resulting images were calibrated using nightly beam maps of Uranus, Mars and occasionally CRL 618. Absolute flux calibration is accurate to 10 and 20 per cent at 850 and $450\ \mu\text{m}$, values fixed in part by the 5-per cent uncertainty in the brightness temperature of Mars. Several calibration methods were employed and used in the appropriate circumstances: the conventional ‘Jy beam $^{-1}$ ’ method was used primarily to calculate the noise in each map; an ‘aperture photometry’ method, with a variety of apertures, was used to measure source flux densities in map regions not affected significantly by confusion. The maps are presented in Fig. 2.

Source catalogues from our fields were constructed using the SExtractor package (Bertin & Arnouts 1996). The detection algorithm requires that the surface brightness in four contiguous pixels (or 64 sq. arcsec) exceeds a threshold after subtracting a smooth background signal and convolving the map with a $16'' \times 16''$ top-hat filter. The detection threshold used was 1σ of the map noise (Table 1), which includes both contributions from sources and their negative reference beams. The ‘true’ map noise is typically 20–30 per cent lower than the values listed in Table 1.

Our observations were obtained early in SCUBA’s operation and we adopted a conservative azimuthal chop, since it was then unclear whether differential spillover of the beam sidelobes onto the ground could lead to systematic errors or increased noise for R.A./Dec.-chopped observations. This is now known not to be a significant effect. The smearing of the negative images of sources in the final map, when using azimuthal chopping, reduces their usefulness for CLEAN-type analyses (Hughes et al. 1998; Ivison et al. 2000b) and our source detection therefore does not use any information from the negative images of sources. Once detected, however, the sources were checked visually: all of the brightest sources have negative counterparts at the expected positions (e.g. for the A 370 map in Fig. 2 these lie $60''$ to the north-west/south-east of each source). The number of independent resolution elements in our survey is about 760, and so no $4\text{--}\sigma$ noise peaks are expected in the catalogue. As a check, we

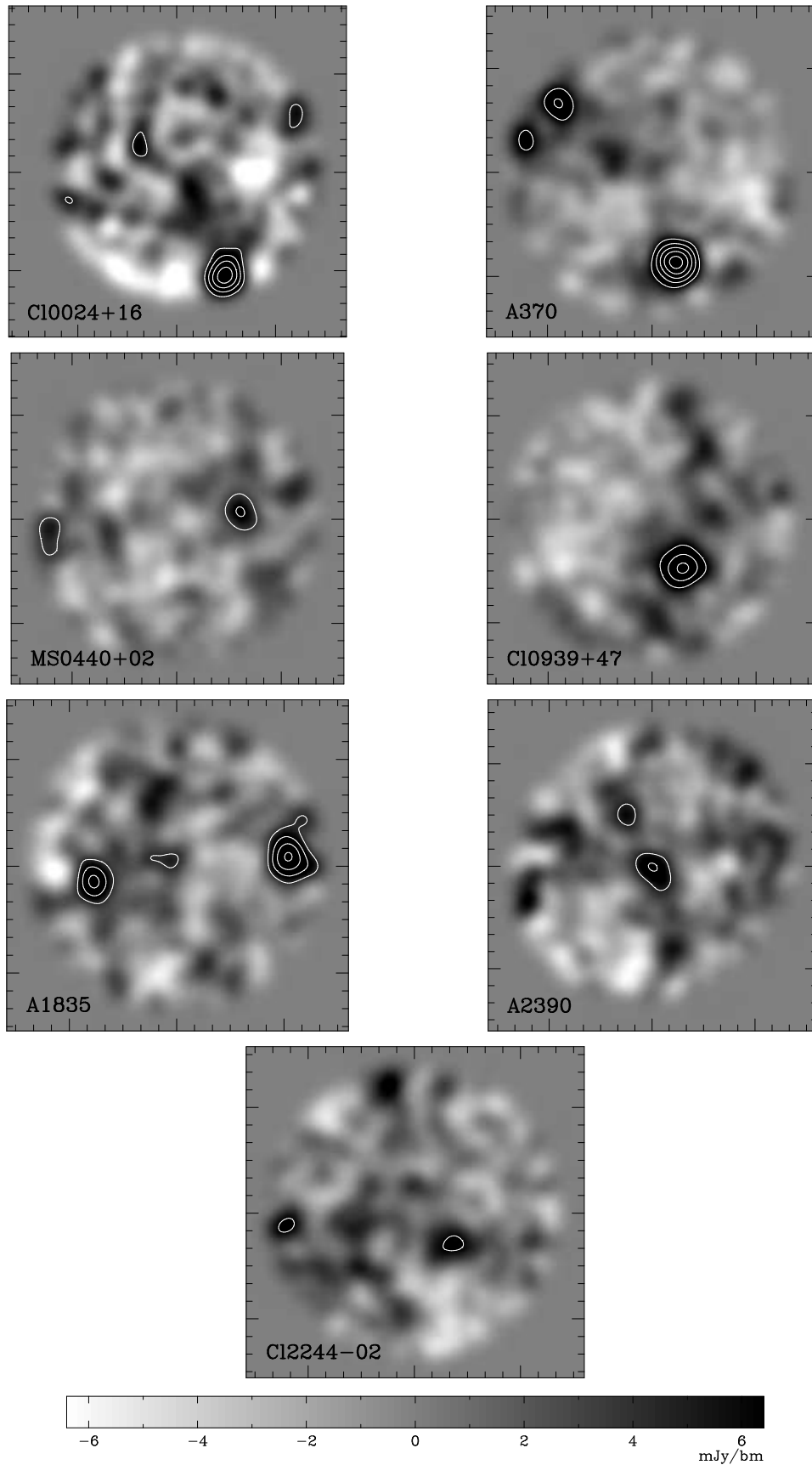


Figure 2. 850- μm maps of the seven cluster fields from the SCUBA Lens Survey. These have been convolved with a 12'' FWHM Gaussian for display purposes and the contours identify the sources in our catalogue. The major tickmarks are every 60'' from the field centre positions given in Table 1. North is up; east to the left. Contours are plotted at $3, 4 \dots \times \sigma$.

ran the detection algorithm on the negative copy of each map and found only the negative reference-beam images of the brightest sources. We were also able to recover all of the sources from independent sub-samples of the data.

As we have not ‘cleaned’ the maps, there is an additional source of confusion for faint sources in those maps which contain at least one bright source: the reference beams from bright sources could be chopped onto another source, resulting in deviations in its apparent position and flux density. However, the only clear case of this is for SMM J14010+0252 (the central galaxy in A 1835), where the chopped images of two bright sources overlap near the central galaxy, both reducing its flux density and confusing its position (Iverson et al. 2000a).

With the lensing amplification taken into account, the data shown in Fig. 2 are some of the deepest sub-mm maps so far published. In regions close to critical lines in the image plane the maps are sensitive to galaxies with intrinsic flux densities as faint as 0.2 mJy, if these have a surface density great enough to populate the relevant regions of the source plane.

A total of 17 sources are detected above the nominal 3- σ limits, and 10 above the 4- σ limits, of the 850- μm maps (which correspond to ~ 4 - and ~ 5 - σ when using noise estimates from cleaner regions of the maps). We list these in order of their fluxes in Table 2. These are detected in a total surveyed area of $\simeq 40 \text{ arcmin}^2$ in the image plane (Fig. 3). None of the sources are resolved at 850 μm (c.f. Iverson et al. 2001a). Five of these sources are also detected at 450 μm (Table 2). From the surface density of sources detected in a typical field, we can be confident that our observations are not limited by confusion: there are ~ 45 beams per source (Blain, Iverson & Smail 1998; Hogg 2001).

The atmospheric transparency at 450 μm on Mauna Kea is lower than at 850 μm even in good weather, and together with the reduced aperture efficiency this explains the smaller number of sources detected in our 450- μm maps (Table 2). The flux density limits for detection in the 450- μm maps are listed in Table 1.

3 SUB-MM SOURCE COUNTS AND THE EXTRAGALACTIC BACKGROUND

Our complete 850- μm sample comprises a total of 17 galaxies, two of which are identified with the central cluster galaxies (cDs) in the clusters A 1835 and A 2390. Edge et al. (1999) provide more discussion of the cDs; we list their properties in Tables 2, 4 and 5 for completeness, but exclude them from our subsequent analysis. Initially, a further two submm sources were associated with galaxies in the foreground of the lensing clusters (Smail et al. 1998); however, additional data has provided more plausible counterparts in the background (§5). Thus all 15 of the non-cD detections appear to be background galaxies.

The analysis of these 15 sources makes use of well-constrained lens models for all the clusters to accurately correct the observed source fluxes for lens amplification. We use the same approach as that employed by Blain et al. (1999a), but include SMM J04431+0210 and SMM J09429+4658 in the analysis, based upon the subsequent identifications of their counterparts as background galaxies. We briefly de-

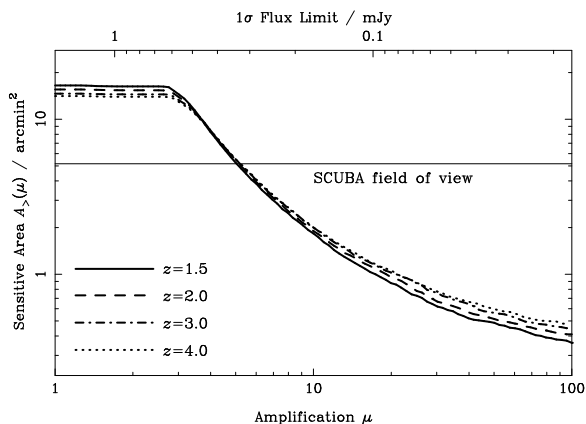


Figure 3. The total area surveyed in the source plane across all seven clusters in our sample as a function of lens amplification and amplification-corrected 850- μm flux density. The latter assumes a typical value of the effective noise in our maps of 1.7 mJy rms. The cluster lenses provide an increasing sensitivity across a decreasing area of the background plane. The effect is mildly dependent on the source redshift. Details of the magnified area for each cluster can be found in Fig. 1 of Blain et al. (1999a).

scribe the method below. The interested reader should refer to Blain et al. (1999a) for more details and references for the lens models employed for specific clusters.

In each cluster we use the appropriate LENSTOOL models (Kneib et al. 1996), to map the detected sources from their observed positions back onto the source plane assuming source redshifts of $z_s = 1.5, 2, 3$ and 4 (this correction varies only slightly for sources at $z_s \gtrsim 1$ and so we have adopted the $z_s = 3$ case, in line with the results discussed in §4.6). The observed flux densities are also corrected for lens amplification, leading to true flux densities in the source plane that are less than the observed values. Note that the amplifications quoted in Table 4 are calculated using the redshift constraints listed in that table, while the calculation here assumes a median redshift for the sample as a whole. None of the SCUBA sources appear to be multiple images (van der Werf et al. 2001b) of the same galaxy (although see SMM J00266+1710 in §5) and so we count them individually. The number counts, $N_{\text{raw}}(> S, z)$, are calculated by simply summing the number of sources brighter than a flux density S in the source plane, after correcting for lensing. A simple approximation to the Poisson uncertainty $1.1\sqrt{N_{\text{raw}} - 1}$ is attached to this value for $N_{\text{raw}} \geq 4$; for $N_{\text{raw}} < 3$, results from Gerhels (1986) are used. Poisson noise due to the modest sample size dominates both calibration uncertainties and uncertainties in the lensing correction.

Next we estimate the area surveyed by our observations. The area of background sky within which a galaxy would be detectable above a given flux limit in each cluster was determined from a map of the amplification in the source plane, derived using the LENSTOOL models. Based on this, the area of the source plane behind each cluster that lies within the SCUBA field of view, and is amplified by a factor greater than μ , $A_{>}$ is shown in Fig. 3. Due to the amplification, $A_{>}$ is smaller than the SCUBA field of view. The uncertainty in the lensing correction of the effective area of the survey is much smaller than the Poisson uncertainty on the

Table 1. Summary of the Observations

Cluster	α, δ (J2000)	z_{cl}	T_{SCUBA} (ks)	$\sigma(850\mu\text{m})$ (mJy)	$\sigma(450\mu\text{m})$ (mJy)	T_{VLA} (ks)	$\sigma(1.4\text{GHz})$ (μJy)	T_{ROSAT} (ks)	$\sigma(1.0\text{KeV})^a$
Cl0024+16	00 26 35.80 +17 09 41.0	0.39	15.6	1.5	20	75.7	15	82.6	2.6
A 370	02 39 53.00 -01 35 06.0	0.37	33.8	1.9	10	65.8 ^b	10	29.7	2.9
MS 0440+02	04 43 09.00 +02 10 19.9	0.19	35.8	1.5	20	27.9	15	27.3	4.2
Cl0939+47	09 42 56.38 +46 59 10.4	0.41	30.1	1.9	7	60.0 ^b	9	45.8	2.7
A 1835	14 01 02.20 +02 52 43.0	0.25	23.0	1.7	7	26.6 ^b	16	2.8	16
A 2390	21 53 36.89 +17 41 45.8	0.23	33.7	2.2	20	9.7	100	32.8	4.0
Cl2244-02	22 47 11.90 -02 05 38.0	0.33	25.6	1.7	20	27.8	17	33.7	3.5

a) $1-\sigma$ flux limits in the 0.1–2.0 keV band from archival *ROSAT HRI* observations, in units of 10^{-15} erg s $^{-1}$ cm $^{-2}$ –
b) excluding A-configuration data (Owen et al., in prep; Ivison et al., 2001b).

Table 2. Catalogue of Source Positions and Submm Fluxes

Source	S_{850} (mJy)	S_{450} (mJy)	Submm α, δ (J2000)	Radio α, δ (J2000)	Opt/NIR α, δ (J2000)	Comments
SMM J02399-0136	23.0	85	02 39 51.9 -01 35 59	02 39 52.00 -01 35 57.9	02 39 51.88 -01 35 58.0	L1/L2 ^a
SMM J00266+1708	18.6	...	00 26 34.1 +17 08 32	00 26 34.06 +17 08 33.1	00 26 34.11 +17 08 33.2	M11 ^{b,g}
SMM J09429+4658	17.2	61	09 42 54.7 +46 58 44	09 42 54.51 +46 58 44.7	09 42 54.65 +46 58 44.7	H5 ^c
SMM J14009+0252	14.5	33	14 00 57.7 +02 52 50	14 00 57.55 +02 52 48.6	14 00 57.57 +02 52 49.1	J5 ^d
SMM J14011+0252	12.3	42	14 01 05.0 +02 52 25	14 01 04.96 +02 52 23.5	14 01 04.97 +02 52 24.6	J1/J2 ^d
SMM J02399-0134	11.0	42	02 39 56.4 -01 34 27	02 39 56.30 -01 34 30.9	02 39 56.51 -01 34 27.1	L3 ^e
SMM J22471-0206	9.2	< 60	22 47 10.4 -02 05 59	...	22 47 10.10 -02 05 57.2	P4?
SMM J02400-0134	7.6	< 50	02 39 57.9 -01 34 45	Blank
SMM J04431+0210	7.2	< 60	04 43 07.2 +02 10 24	...	04 43 07.10 +02 10 25.1	N4 ^c
SMM J21536+1742	6.7	< 60	21 53 38.2 +17 42 13	...	21 53 38.31 +17 42 13.3	K2?
SMM J00265+1710	6.1	< 60	00 26 31.3 +17 10 04	00 26 31.28 +17 10 09.6	...	Blank?
SMM J22472-0206	6.1	< 60	22 47 13.9 -02 06 11	...	22 47 13.76 -02 06 07.9	P2?
SMM J00266+1710	5.9	< 60	00 26 37.9 +17 09 51	Blank?
SMM J00267+1709	5.0	< 60	00 26 39.7 +17 09 12	Blank
SMM J04433+0210	4.5	< 60	04 43 15.0 +02 10 02	04 43 15.04 +02 10 01.3	04 43 15.06 +02 10 02.8	N5
Cluster Galaxies						
SMM J21536+1741	9.1	< 30	21 53 36.9 +17 41 42	21 53 36.81 +17 41 43.5	21 53 36.74 +17 41 44.2	A 2390 cD ^f
SMM J14010+0252	5.4	20	14 01 02.3 +02 52 40	14 01 02.09 +02 52 42.6	14 01 02.11 +02 52 43.1	A 1835 cD ^f

a) Ivison et al. (1998a) – b) Frayer et al. (2000) – c) Smail et al. (1999a) – d) Ivison et al. (2000a) – e) Soucail et al. (1999) –
f) Edge et al. (1999) – g) Falls outside the 450- μm map.

counts. We have verified that this is case by assuming different source redshifts between $z = 1.5$ and 4, as shown in Fig. 3.

To calculate the effective area of our survey to a given sensitivity limit we use the fact that a galaxy with a flux density S in the source plane will appear in the image plane of a particular cluster above a detection threshold S_{min} if it is amplified by a factor greater than $\mu = S_{\text{min}}/S$. The area in the source plane within which such a galaxy would be detected in that cluster is then $A_{>}(S_{\text{min}}/S, z)$. The flux density threshold S_{min} and the form of $A_{>}$ are different for each cluster. By dividing the number of detected galaxies in the catalogue N_{raw} by the sum of the areas $A_{>}(S_{\text{min}}/S, z)$ for all seven clusters, the count $N(> S, z) \simeq N_{\text{raw}}(> S, z) / \sum A_{>}(S_{\text{min}}/S, z)$ is derived.

The final 850- μm counts are shown in Table 3 and Fig. 4. These are within the $1-\sigma$ errors of our previous anal-

ysis of the 850- μm counts (Blain et al. 1999a). The results are thus insensitive to the precise identification of individual submm sources in our survey.

The effects of uncertainties in the redshift distribution of the sources for the lensing reconstruction, and hence for the final counts, were quantified by adopting different assumed source redshifts, as illustrated in Fig. 2 of Blain et al. (1999a). The uncertainty is less than about 10 per cent, and is dominated by the Poisson noise. An appropriate systematic uncertainty term is included in the counts listed in Table 3 and shown in Fig. 4. The robustness of our amplification correction was verified by extensive Monte-Carlo simulations (see Blain et al. 1999a). We include the uncertainties associated with our lensing analysis in the final error quoted on the counts listed in Table 3. The total uncertainty in the lensing correction is at most comparable to the typical 10-per-cent error in the absolute flux calibration.

We have applied the same methods to the catalogue constructed from the 450- μm maps of the seven lensing clusters observed in the survey (Blain et al. 2000). The 450- μm counts that result from the analysis are listed in Table 3 and Fig. 4.

The 15 sources detected at 850 μm in this survey suffer a range of lens amplifications, $1.5 \lesssim 4$ (Table 4). For the median source amplification of ~ 2.5 (Fig. 3) our survey covers an area in the source plane equivalent to $\sim 15 \text{ arcmin}^2$ to a $3\text{-}\sigma$ flux density limit of about 2 mJy at 850 μm . At higher amplifications, the survey covers a smaller region at a correspondingly higher sensitivity, in particular regions of very high amplification lie within our survey areas along critical lines. As a result, we are able to constrain the general form of the integral counts at even fainter limits, down to $\lesssim 0.5$ mJy, because we know the area in the source plane over which such faint sources could be detected, and the number of sources brighter than this limit that were detected.

The absolute limit to the depth of the survey can be determined from Fig. 3, which shows that a significant area behind the cluster lenses is surveyed down to the 0.25 mJy $3\text{-}\sigma$ flux density level – approximately 0.7 arcmin^2 , or about 10 observing beams on the sky. Note that the lens amplification in the cluster fields also results in an effective beam size that is about half the size of the apparent beam, enabling a fainter confusion limit to be reached as compared with blank-field observations (see §3.1 and Fig. 5). However, fainter than about 0.25 mJy the effects of source confusion, and the uncertainty in the area of the high-magnification region shown in Fig. 3 are likely to become significant, and so we plot the derived counts from the direct inversion technique as an upper limit at 0.25 mJy. This limit is consistent with the lack of any clear candidates for multiply-imaged submm sources amongst the sources with typical fluxes of 4–5 mJy in the catalogue. The magnification of such multiply-imaged systems is expected to be in excess of 10, and so it is reasonable to quote only an upper limit at a flux density of 0.25 mJy, which is a factor of 20 deeper than the faintest source. We note, however, that this constraint may be strengthened by future submm surveys of clusters lenses. In particular, van der Werf et al. (2001b) have recently detected a multiply-imaged, and thus highly amplified, submm source in A 2218.

While both the results of the direct inversion technique and the Monte Carlo method are of course uncertain, due to the unknown redshifts of a fraction of the sources – they give consistent results at flux densities fainter than 1 mJy (Fig. 4). Both techniques suggest that at least one, and probably several, of the four sources with lower limits on their amplifications actually arises from the 0.5–1 mJy population. Correlation of fainter features in the submm maps with multi-waveband data in the radio, X-ray and mid-IR, can be used to identify examples of the sub-mJy submm population (Ivison et al. 2000a; Fabian et al. 2000).

Our Monte Carlo method (Blain et al. 1999a) yields a count of the form $N(> S) = K(S/S_0)^\alpha$ as a function of flux density S . At 450 μm , $K = 530 \pm 300 \text{ deg}^{-2}$ and $\alpha = -1.8 \pm 0.5$ for $S_0 = 20$ mJy. At 850 μm , $K = 3900 \pm 1300$ and $\alpha = -1.4 \pm 1.0$ for $S_0 = 2$ mJy. The envelopes of these results are shown by dashed lines in Fig. 4, which show that an approximate power-law count provides a reasonable description of the cumulative count in the flux density ranges plotted. The equations describing these lines at 450 and

Table 3. Submm counts at 450 and 850 μm . The third column lists the results from the current analysis. The fourth column lists the earlier results from Blain et al. (1999a).

Band (μm)	Flux (mJy)	Cumulative Count (10^3 deg^{-2})	Blain et al. (1999a) (10^3 deg^{-2})
450 μm	10.0	2.1 ± 1.2	...
	25.0	0.5 ± 0.5	...
850 μm	0.25	51 ± 21	...
	0.5	27 ± 10	22 ± 9
	1.0	9.5 ± 3.4	7.9 ± 3.0
	2.0	2.9 ± 1.1	2.6 ± 1.0
	4.0	1.7 ± 0.8	1.5 ± 0.7
	8.0	0.90 ± 0.58	0.8 ± 0.6
	16.0	< 0.42	...

850 μm both have $\alpha = -1.6$. For $S_0 = 25$ mJy at 450 μm , $K = 480 \text{ deg}^2$; for $S_0 = 3$ mJy at 850 μm , $K = 2000 \text{ deg}^2$.

We estimate that the flux density in the resolved submm population down to 1 mJy at 850 μm amounts to a background radiation intensity $I_\nu = (3 \pm 1) \times 10^{-10} \text{ W m}^{-2} \text{ sr}^{-1}$, while at 450 μm , $I_\nu = (7 \pm 4) \times 10^{-10} \text{ W m}^{-2} \text{ sr}^{-1}$ down to 10 mJy. Note that this procedure simply involves adding the detected flux densities of the non-cluster galaxies in our survey. Gravitational lensing does not modify surface brightness, and so there is no need for any amplification correction. The uncertainties in this procedure are entirely due to the limited size of the sample, the calibration uncertainties in the SCUBA images and cosmic variance. Compared to the total intensity of extragalactic background radiation at these two wavelengths, measured using *COBE*-FIRAS (Fixsen et al. 1998), we resolve about 60 and 15 per cent of the 850- and 450- μm backgrounds down to flux densities of 1 mJy and 10 mJy respectively (see Fig. 4). Unless the counts flatten rapidly below 1 mJy, the bulk of the 850- μm background will be resolved at flux limits of 0.1–0.5 mJy (Hughes et al. 1998).

A typical galaxy in our sample has an intrinsic 850- μm flux density of 3–4 mJy after correcting for lensing (see Table 4). From Fig. 1, it is clear that if these galaxies lie at $z \gtrsim 1$, and provided that their temperatures are not substantially less than 40 K, then all are ULIRGs, with far-IR luminosities $L_{\text{FIR}} \gtrsim 10^{12}\text{--}10^{13} L_\odot$. There is no evidence that either of these conditions is breached for any of our submm-selected galaxies. Even in low-redshift low-luminosity *IRAS* galaxies for which submm data is available (Dunne et al. 2000; Lisenfeld, Isaak & Hills 2000), the mean temperature is 36 K (but see Dunne & Eales 2001), and there is a general trend for more luminous objects to have higher dust temperatures. Thus we can conclude that at least half of the submm background is produced by ULIRGs ($L_{\text{FIR}} \geq 10^{12} L_\odot$, equivalent to flux densities ≥ 1 mJy), with the bulk of the remainder coming from LIRGs (Sanders & Mirabel 1996; $L_{\text{FIR}} \geq 10^{11} L_\odot$). Hence, most of the submm background is produced by galaxies with a relatively narrow range of luminosities, in contrast with the very wide luminosity range contributing to the optical and near-IR backgrounds.

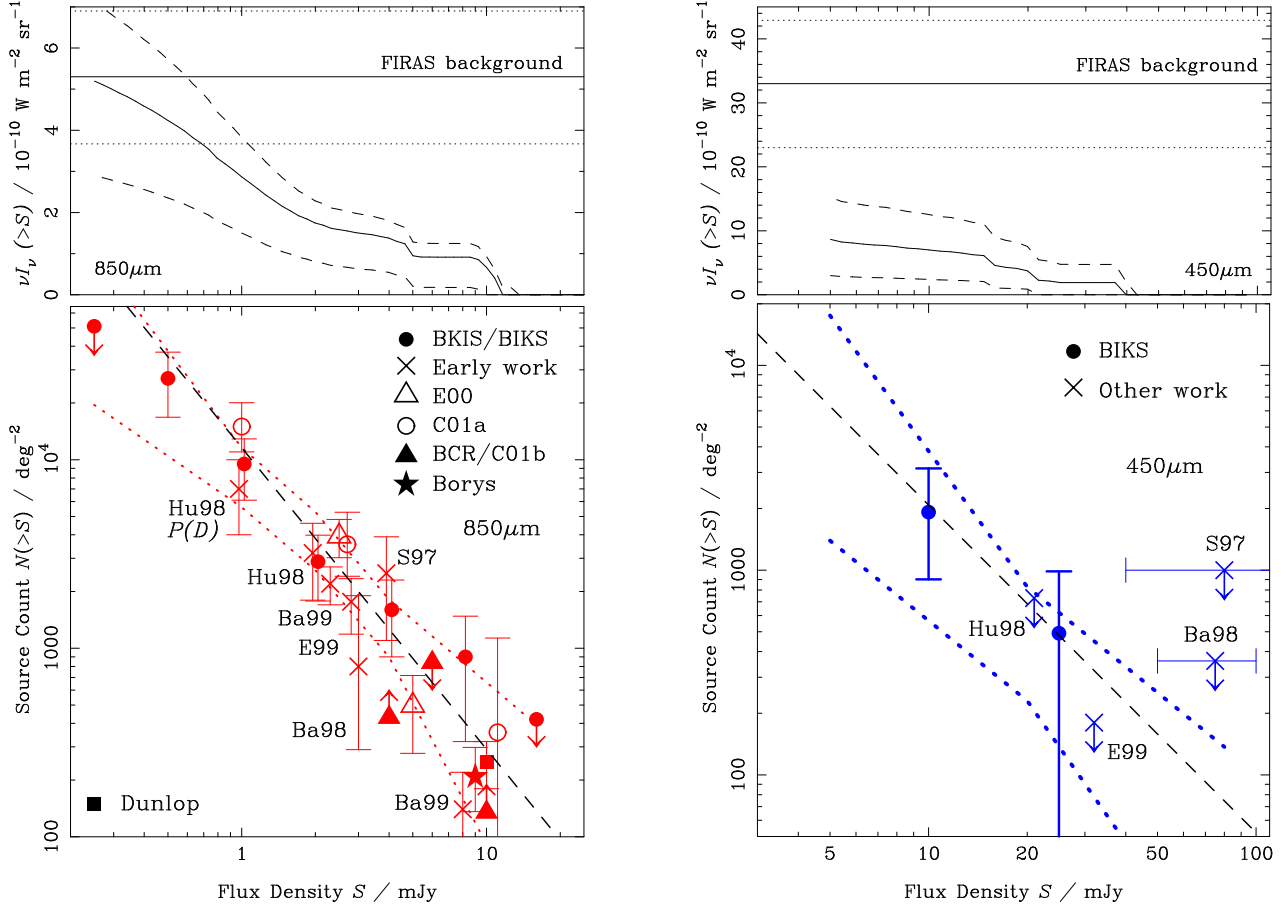


Figure 4. **Left:** the 850- μm counts of galaxies, including the updated SCUBA Lens Survey counts (corrected for lens amplification). To avoid complicating the figure, the direct counts obtained by Blain et al. (1999a; see Table 3) are not shown. The associated Monte-Carlo results are shown by the dotted lines. Ba98/Ba99 – Barger et al. (1998, 1999a); E99 – Eales et al. (1999); Hu98 – Hughes et al. (1998); S97 – Smail et al. (1997). The latest counts from Eales et al. (E00, 2000), Borys et al. (2001), Chapman et al. (C01a, 2001a) and Dunlop (2001) are also shown. Limits from submm-wave observations of infrared-faint radio-selected objects (Barger, Cowie & Richards – BCR – 2000; Chapman et al. – Co1b – 2001b) are also included. To avoid overcrowding only the faintest and brightest results from non-cluster surveys are plotted on the figure. The top panel compares the cumulative flux in the resolved population from a direct integration of our counts to that estimated by *COBE*. **Right:** the equivalent 450- μm counts of galaxies. The direct and Monte Carlo counts derived here are shown by the solid points and dotted lines respectively. The dashed line gives the parametric fit to the counts quoted in the text. Again the top panel shows the flux of the resolved population compared to the estimate of the total background given by *COBE*.

3.1 Confusion in SCUBA surveys

Unresolved and undetected faint sources in the large SCUBA beam generate an additional source of noise in survey maps. Estimates of the magnitude of this effect were presented by Blain et al. (1998), based on the results obtained early in the SCUBA Lens Survey. The noise properties of the SCUBA map of the HDF (Hughes et al. 1998) clearly shows a non-Gaussian tail characteristic of this effect, illustrated in their Fig. 5.

Here we simulate confusion for SCUBA by drawing a large number of simulated background galaxy distributions from the counts shown in Fig. 4. We then simulate the observation of these fields using the standard $-0.5/+1/-0.5$ SCUBA chopping scheme and resolution. The distribution of measured values in the absence of additional instrumental and sky noise is shown in Fig. 5a, while the effects of adding additional Gaussian noise with a variance of 1.7 mJy, characteristic of the effective noise level in the Lens Survey, is shown in Fig. 5b. The smooth Gaussian profile superimposed

on Fig. 5a has the same width as the estimate of confusion noise (0.44 mJy) presented by Blain et al. (1998). In Fig. 5b the smooth profile represents a Gaussian of width 1.7 mJy, describing the non-confusion noise. Note that the distribution of flux densities shown should apply to every point in the sky, both those containing detected sources and those without.

The non-Gaussian properties of the confusion signal are clearly visible in Fig. 5a. The core of the distribution is well described by a Gaussian, but there is a long high-flux tail that is not accounted for by this distribution. The distribution is also noticeably asymmetric, although the asymmetry is reduced by the three-position chopping scheme. A log-normal distribution can provide a good description of the high-flux tail; however, it is clear from the distribution of simulated measurements that confusion is unlikely to be severe at flux densities greater than 2 mJy. In Fig. 5b, the additional noise sources swamps the confusion signal, and the noise properties are almost Gaussian.

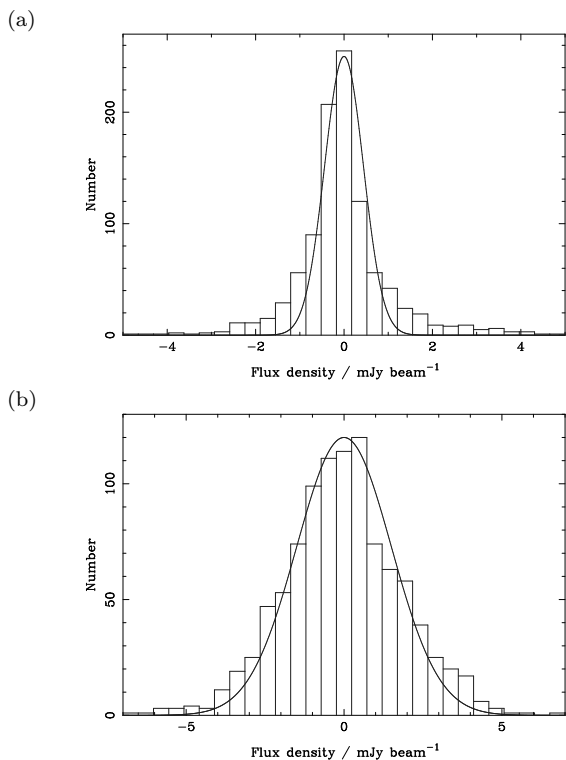


Figure 5. Simulated levels of source confusion in SCUBA mapping observations. In (a), the asymmetric confusion noise distribution in chopped observations in the absence of instrumental or sky noise are shown by the histogram. The smooth curve has a width corresponding to the estimate of confusion noise in Blain et al. (1998). There is an additional non-Gaussian tail to the distribution. In (b), the results of similar simulations are shown, with an additional 1.7-mJy Gaussian noise source added, typical of the depth of the SCUBA Lens Survey observations. The effect of confusion is very small, as the solid curve representing the additional sky and instrument noise is very similar to the histogram.

Recently, Hogg (2001) simulated the effects of confusion for reliable determination of source positions and fluxes in 850- μm SCUBA surveys, arguing that for reliable detections, a limit of about 2 mJy is required for a count with $N(> S) \propto S^{-1.5}$, in agreement with the result above. In contrast, Eales et al. (2000) have argued that confusion biases the positions and especially the fluxes of sources at brighter levels, $\gtrsim 3\text{--}4$ mJy. The simulations of Eales et al. (2000) appear to assume a very steep integral count slope of $N(> S) \propto S^{-2.6}$, based on their Fig. 3, than found here. This count is significantly steeper than the envelope of all the current counts shown in Fig. 3. Because the effects of confusion are more severe for steeper counts (see Figs 2, 3 & 4 in Hogg 2001), this assumption of Eales et al.’s simulations is likely to account for the difference with our results. The estimates of the positional uncertainty of sources due to confusion, from both the Eales et al. and Hogg simulations, confirm that sources can easily move by at least half the beamwidth due to shifts in image centroids imposed by underlying confusing sources.

Based on the counts shown in Fig. 3, at the 3–4 mJy depths involved in the SCUBA Lens Survey, and the CFRS survey, confusion is unlikely to be significant compared with instrument and sky noise, unless the data are smoothed.

The typical effect of confusion at these flux densities is to disperse measured source flux densities by of order 0.5 mJy, slightly increasing the number of formal detections at the faintest levels. Neither of these effects would significantly modify our results, and would certainly not lead to a uniform boosting of the flux density of all the detections by 40 per cent as claimed by Eales et al. (2000). No systematic boost of the flux density of sources at all observed fluxes was found here or in the results shown in Fig. 3 of Hogg (2001). However, for very steep counts, which may well occur at flux densities in excess of 20 mJy, then significant flux boosting of this kind can certainly occur. The effects of confusion in the existing SCUBA surveys should be easy to quantify when accurate flux densities and positions for SCUBA sources are determined using submillimeter interferometers such as the forthcoming Submillimeter Array (SMA; Ho et al. 2000).

4 IDENTIFYING COUNTERPARTS TO SUBMM SOURCES

Having resolved the majority of the 850- μm background we can now move on to attempt to study the nature of the populations contributing to it and so determine at what epoch the background was emitted. Here again our survey has the advantage of lens amplification, this time in the radio and optical/near-IR where the identification and spectroscopic follow-up are undertaken. Typically the counterparts of our submm sources will appear ~ 1 mag. brighter than the equivalent galaxy in a blank field, providing a gain equivalent to moving from a 10-m to a 16-m telescope.

However, the low spatial resolution of SCUBA on the JCMT, $15''$ at 850 μm , combined with the faintness of the counterparts to the submm sources in most other wavebands, can make identification of counterparts on the basis of positional coincidence difficult. The absolute astrometry of the submm maps is not an issue with these comparisons – it has been confirmed for several of the brighter sources using mm-wave interferometry (Frayer et al. 1998, 1999, 2000; Ivison et al. 2001b; Kneib et al. 2002; §4.3; see also Downes et al. 1999; Gear et al. 2000; Bertoldi et al. 2000; Lutz et al. 2001). These observations confirm that the typical random astrometric errors for bright submm sources is $\lesssim 2\text{--}3''$, this is expected to degrade to $\sim 4''$ for the faintest sources in our sample (see Hogg 2001).

In the remainder of this section we chart the chronological development of our source identification process to illustrate how it has evolved over the lifetime of the project.

4.1 Optical counterparts

Although the submm galaxies are expected to be very dusty, it is not foregone conclusion that they will be either very red or optically faint – the restframe UV colours of local ULIRGs span a wide range and include examples of relatively blue galaxies (Trentham et al. 1999; Fig 8). We therefore began our search for counterparts of the submm sources in our survey in the optical waveband.

One of the key features used in selecting the SCUBA survey clusters for this study was that they were well studied, and in particular that deep, high-quality archival optical

imaging existed for each of the fields, including *Hubble Space Telescope (HST) WFPC2* imaging.

Details of the optical observations, their reduction and analysis can be found in Smail et al. (1998). More detailed discussion of the optical observations of specific fields is given by Ivison et al. (1998a) and Soucail et al. (1999) for A 370 by Ivison et al. (2000a, 2001b) for A 1835 and by Smail et al. (1999a) for the MS 0440+02 and Cl 0939+47 fields.

All the frames are calibrated to provide standard Cousins *I*-band photometry and are linked astrometrically to the APM coordinate system with a typical accuracy of $\lesssim 0.5''$. Colours are measured using $2''$ -diameter apertures from the seeing matched *I*- and *K*-band frames (Table 4). When total *I*-band magnitudes are quoted these refer to $4''$ -diameter aperture photometry corrected for light falling outside the aperture assuming a point source profile.

We show in Fig. 6 the submm maps of each of the 15 cluster background sources overlaid on the deep *I*-band exposures of these frames. For the sources in A 2390, Cl 2244–02 and most of those in Cl 0024+16, we use *HST* F814W (*I*) images degraded to the same seeing and pixel scale as ground-based near-IR images (see §4.2). For the remaining fields we have used deep, ground-based *I*-band frames: for Cl 0939+47 and MS 0440+02 we use the Keck *I*-band imaging from Smail et al. (1999a) and for A 1835 and A 370 the Hale 5-m and CFHT imaging discussed in Smail et al. (1998).

However, in the course of this analysis it has become clear that identifying submm counterparts using optical data *alone* is a problematic process (Smail et al. 1998; Lilly et al. 1999). With the exception of a handful of three unusual and optically-bright counterparts: SMM J02399–0136 (Ivison et al. 1998); SMM J02399–0134 (Soucail et al. 1999) and SMM J14011+0252 (Ivison et al. 2000a), the majority of the submm sources cannot be reliably identified on the basis of just optical imaging, irrespective of its depth (§4.6; Smail et al. 2000).

4.2 Near-infrared counterparts

To more reliably identify counterparts to the 15 submm sources we next obtained near-IR imaging of our fields. The goal is to combine this with the deep optical data, to attempt to locate any counterparts within the submm error box on the basis of their unusual optical–near-IR colours, e.g. $(I - K) \gtrsim 5$. For this purpose the depth required in the *K*-band was set by the depth of the available *I*-band images, $I \sim 25$ – 26 , with the deepest being the multi-orbit *HST* exposures, leading to a limit of $K \sim 20$ – 21 for our observations. In most cases, integrating fainter in *K* might produce additional candidate counterparts but we would be unable to identify these as unusual on the basis of their very red colours from our existing optical images. In the few cases where more accurate positional information about a probable submm source is available, from either mm-wave continuum or radio interferometry maps, deeper *K*-band observations have been obtained (e.g. Ivison et al. 2000a; Frayer et al. 2000).

The near-IR observations of our fields were undertaken in typically good conditions during several observing runs in late 1998 and early 1999 using the IRCAM3 and UFTI

cameras on the 3.8-m UKIRT[‡]. Observations consist of deep *K*-band exposures (with *J*- or *H*-band observations of the brighter sources detected in *K*).

Data were obtained with IRCAM3 on the nights of 1998 July 11–16 and 18, September 10 and 19, October 9 and 1999 February 8–12. The new UFTI camera, which provides finer sampling of the average seeing on UKIRT, was used on 1998 October 18–19 and November 19. The seeing during these nights was typically 0.4 – $0.8''$. Data taken in non-photometric conditions (1998 July 16, September 19 and October 18–19) were calibrated using independent exposures taken on photometric nights. Total exposure times for the individual fields are listed in Table 4.

Observations of the MS 0440+02 and Cl 0939+47 fields are discussed in Smail et al. (1999a), while Ivison et al. (1998a, 2000a) discuss the A 370 and A 1835 fields, respectively. Frayer et al. (2000) present very deep near-IR observations of SMM J00266+1708. Here we describe the results for the complete sample. We note that a programme of deeper near-IR imaging and spectroscopy, targeting the brightest submm sources, is currently underway on Keck to attempt to identify faint near-IR counterparts in some of the blank or ambiguous fields (see Frayer et al. 2000 for the first results).

The UKIRT observations used repeated sequences of nine exposures dithered on a 3×3 grid with a $10''$ separation to allow the science images to be flatfielded using a running median sky frame constructed from the adjacent science frames. The frames were linearised, dark subtracted, flatfielded and combined in a standard manner. The final stacked frames were photometrically calibrated using UKIRT Faint Standards (Casali & Hawarden 1992). The astrometry on these frames comes from comparison with the *I*-band exposures of these fields.

We show in Fig. 6 *K*-band images of the fields of the sources and compare these to the *I*-band images to illustrate the colours of possible counterparts. In combination with the deep optical data, it is simple to pick out several unusually red galaxies, which are bright in the *K*-band and faint or undetected in the *I*-band. Of these, amongst the most striking are the extremely red objects (EROs, e.g. Smith et al. 2001b) in the fields of SMM J09429+4658 and SMM J04431+0210 (§5). The low surface density of such very red galaxies in blank fields, combined with the possible connection between their extreme colours and the presence of dust, both argue for these galaxies being the correct counterparts to the submm sources (see Smail et al. 1999a).

From the near-IR imaging of our complete submm sample, which reaches a median 2σ depth of $K \sim 21$ ($K \sim 22$ in the source plane), we identify counterparts to about half of the submm sources in the sample, of these around half again are also visible in the optical. Table 4 lists photometry for the various counterparts and we discuss these further in §5. In Table 4, a non-detection corresponds to the 2σ limit on the total magnitude of a point source.

[‡] UKIRT is operated by the Joint Astronomy Centre on behalf of the Particle Physics and Astronomy Research Council of the United Kingdom.

4.3 Radio counterparts

Deep radio maps provide the most powerful complement to our submm observations. This is particularly true of observations at 1.4 GHz from the NRAO Very Large Array[§] (VLA). The resulting maps are sensitive to star-forming galaxies out to high redshifts (e.g. Richards 1999; Smail et al. 1999b), have a spatial resolution that is well matched to the expected size of distant galaxies, and high astrometric precision; they thus provide the best opportunity to unambiguously identify the counterparts of submm sources (Ivison et al. 1998a, 2000a, 2001b).

The deep 1.4-GHz maps used by Smail et al. (2000) to identify radio counterparts for the submm sources in our sample were all obtained with the VLA in A and/or B configuration, giving effective resolutions of 1–5". In A configuration, most of the detected galaxies are resolved, some more than others: for SMM J02399–0136 at $z = 2.80$ the two interacting/merging components, L1 and L2, are resolved from each other, and resolved individually (Ivison et al. 1999; Owen et al., in prep). While for SMM J14011+0252 the combined A+B configuration map constructed by Ivison et al. (2001b) resolves the starburst region and shows that it is distinct from the optically-luminous components of this system. In contrast the B configuration maps may provide a more reliable measure of the total radio flux in these extended systems, and hence a better comparison to large-aperture submm fluxes. We list the total exposure times and 1- σ sensitivity limits of the maps in Table 1. The typical 3- σ sensitivity of these deep maps on the background source plane is about 18 μ Jy, and so the sensitivity is sufficient to detect a ULIRG at a redshift $z \simeq 3$ (Downes et al. 1999).

A summary of these observations is given by Smail et al. (2000). More details of the reduction and analysis of individual maps can be found in the following references: for Cl0024+16 in Morrison (1999); for A 370 in Ivison et al. (1998a); for MS 0440+02 in Smail et al. (1999a); for Cl0939+47 in Smail et al. (1999a, 1999b); for A 1835 in Ivison et al. (2000a, 2001b); and for A 2390 in Edge et al. (1999). Note that the bright radio source associated with the central cluster galaxy in A 2390 reduces the sensitivity of the map of this field.

Smail et al. (2000) searched for radio counterparts within the nominal error boxes of the submm sources. In ambiguous cases where the nominal error box is blank in the radio, but a radio source is visible just outside, they adopted the conservative approach of using the flux of that source as a limit on the radio counterpart. When using the radio and submm fluxes to place limits on the possible redshifts of the sources, this approach leads to a firm lower redshift estimate for the submm source (see §4.6).

Using the radio maps, Smail et al. (2000) found counterparts to roughly half the sample (Table 4). Several of these correspond to previously identified counterparts from the optical or near-IR identification campaigns. However, a number were new identifications and these prompted further, deeper near-IR observations using the improved posi-

tions from the radio maps to attempt to detect counterparts (e.g. SMM J14009+0252, Ivison et al. 2000a).

We list the apparent radio fluxes or 3 σ limits in Table 5. For the 10 submm sources with radio counterparts, we measure a median positional offset of only 2.0" between the submm and radio positions. This supports the estimates of the positional accuracy of the submm sources, < 2–4", quoted in §2 and used in the searches for optical and near-IR counterparts (Smail et al. 1998; §4). We note that the good positional accuracy of our submm sources confirms that confusion is not a significant concern for our survey (c.f. Eales et al. 2000).

4.4 Mid-IR properties

Several of the cluster lens targeted by our SCUBA survey have also been imaged in the mid-infrared (mid-IR) using *ISOCAM*. Maps of A 370 and A 2390 at 15 μ m are discussed by Altieri et al. (1999) and Metcalfe et al. (1999), while similar observations have been obtained for Cl 0024+16 and Cl 2244–02 (L. Metcalfe, priv. comm.). In total there are five submm sources in A 370 and A 2390, and if we discount the central galaxy in A 2390 (which is detected by *ISO*, Edge et al. 1999), we find that three of the remaining four submm sources are detected in the *ISO* 15- μ m maps: SMM J02399–0136 (Ivison et al. 1998a), SMM J02399–0134 (Soucail et al. 1999) and SMM J21536+1742, at apparent flux limits of ~ 0.2 –2 mJy. This implies that a minimum of 20 per cent of the submm population (and possibly up to 75 per cent) have 15- μ m counterparts. A similar rate of correspondence between the two populations, 20 per cent, was found by Hughes et al. (1998) in the HDF, with Eales et al. (2000) finding a slightly lower rate (10 per cent) in their sample.

The long-wavelength photometer, *ISOPHT*, was also used to produce 175- μ m maps of three of the fields included in our survey: A 370, Cl 2244–02 and MS 0440+02 for the programme RIVISON/CLUSTERS. Despite long exposure times and large maps, not even the brightest sources in these fields (e.g. SMM J02399–0136) were detected at 3- σ flux limits of ~ 150 mJy.

4.5 X-ray properties

X-ray observations of the submm galaxies provide a useful addition to our view of this population, in part because of the ability of hard X-ray photons produced by AGN to escape from obscured environments. X-ray data can thus be used to search for obscured AGN in the submm population which might be partly responsible for the extreme luminosities of these sources. For this reason there has been considerable interest in obtaining hard X-ray observations of the submm population (Almaini, Lawrence & Boyle 1999; Gunn & Shanks 2001).

The high resolution X-ray imaging capabilities of the *Chandra* X-ray satellite make it well suited to tackle this problem. In contrast, although it has a much higher sensitivity to hard X-rays, data from *XMM/Newton* are less ideal for the cluster fields studied here – the lower spatial resolution making it difficult to detect any emission from the submm galaxies above the strong cluster X-ray emis-

[§] The National Radio Astronomy Observatory is a facility of the National Science Foundation, operated under cooperative agreement by Associated Universities, Inc.

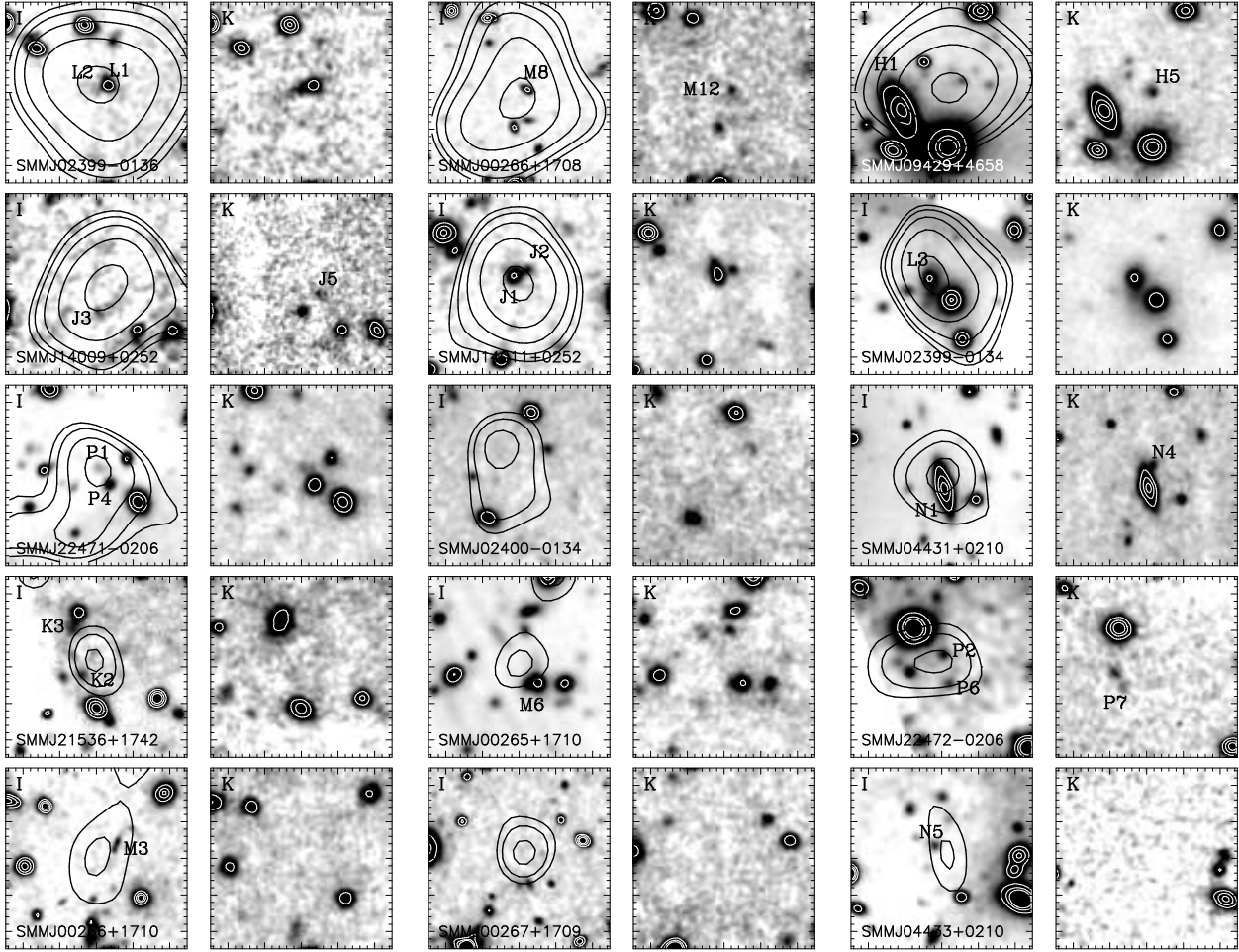


Figure 6. *I*- and *K*-band frames of the fields of the submm sources in our sample (excluding the two central cluster galaxies), ordered in terms of their apparent $850\text{-}\mu\text{m}$ fluxes. The $850\text{-}\mu\text{m}$ map of each source is overlaid as a contour plot on the *I*-band frame, after convolution with an $8''$ -FWHM gaussian for display purposes. Note that the *I*- and *K*-band frames represent a range in depth and resolution, but they have all been smoothed (with a $0.5''$ -FWHM Gaussian) to enhance the visibility of faint features. We identify the various confirmed or candidate counterparts and other galaxies discussed in the text on the individual panels. Each panel is $25''$ -square and has north top and east to the left.

sion. Fabian et al. (2000) discuss sensitive *Chandra* observations of the submm sources in our A 1835 and A 2390 fields, while Bautz et al. (2000) present somewhat deeper observations of A 370. Excluding the central cluster galaxies, these observations cover six of the submm sources in our sample; of these, only two are detected, both of which were already known to host semi-observed AGNs on the basis of their optical and mid-IR emission (SMMJ02399–0136 and SMMJ02399–0134).

To extend this analysis to our full sample we have also made use of deep archival *ROSAT HRI* images of all our fields. Details of the exposure times and sensitivities of the *ROSAT* observations are given in Table 1. These lack both the sensitivity and coverage of the hardest X-ray energies compared to the recent *Chandra* observations; nevertheless, they do allow us to place limits on the presence of strong X-ray emission for *all* of the sources in our sample. We find that no sources have detectable X-ray counterparts down to $3\text{-}\sigma$ flux limits of $\sim 3 \times 10^{-15} \text{ ergs s}^{-1} \text{ cm}^{-2}$ in the $0.1\text{--}2.0 \text{ keV}$ band (roughly $0.4\text{--}8 \text{ keV}$ in the rest frame for most of these sources) after correcting for Galactic HI absorption. At a

redshift of $z \sim 3$ this translates into an X-ray luminosity in the $2\text{--}10 \text{ keV}$ band of $L_X \sim 3 \times 10^{43} \text{ ergs}$, assuming an unobscured $\Gamma = 2$ power-law SED (see the discussion in Bautz et al. 2000).

4.6 Redshift constraints

Constraining the redshifts of possible submm counterparts can also provide a useful route to identifying the correct counterpart to the submm source. These constraints can come from either classical spectroscopy (Barger et al. 1999a) or photometric techniques employing optical, near-IR and longer wavelength observations (e.g. Hughes et al. 1998; Lilly et al. 1999; Smail et al. 2000). Moreover, determining the redshift distribution of the submm population is also important to provide a better understanding of the nature of these galaxies, their relationship to other classes of high-redshift source and their importance for models of galaxy formation and evolution. This is especially important for submm-wave surveys, as the selection function is extremely broad, and so

a priori very high redshift galaxies could be included in the sample.

4.6.1 Optical photometry

Photometric redshift techniques based on optical/UV photometry have been employed by Lilly et al. (1999) to attempt to determine the redshifts of candidate optical counterparts found within the positional error box of submm sources. The results suggested that the bulk of the submm population lies at $z = 0.1\text{--}3$. Hughes et al. (1998) used a photometric technique spanning a larger wavelength range and deduced a range of $z = 2\text{--}4$. Such analyses are based on template spectral energy distributions (SEDs) of local optically-selected galaxies, as sampled in the rest-frame UV waveband if the galaxies are at high redshifts. The diversity of the rest-frame UV/optical properties of even local ULIRGs (Trentham et al. 1999) indicates that such analyses, which employ SED templates derived from ‘normal’ galaxies, are unlikely to be reliable. The SEDs of SCUBA galaxies with known redshifts (Ivison et al. 1998a, 2000a; Soucail et al. 1999) are also diverse and unusual, while the many very red counterparts (Smail et al. 1999a; Dey et al. 1999; Ivison et al. 2000b; Gear et al. 2000; Lutz et al. 2001) would not be well described by standard photometric redshift templates.

4.6.2 Optical spectroscopy

If optical counterparts could be identified for most submm sources then obviously optical spectroscopy would provide the most direct route to obtain the redshift distribution of the population, $N(z)$. Based on the list of plausible optical counterparts from Smail et al. (1998), a spectroscopic survey was undertaken with the Keck telescope (Barger et al. 1999a).

Identifications were attempted for all the galaxies bright enough for reliable spectroscopy within the SCUBA error circles. This resulted in spectroscopic redshifts or limits for 24 possible counterparts to 14 SCUBA sources (SMM J04433+0210 and the two central cluster galaxies were omitted from the survey). The median I -band magnitude of the counterparts is $I = 22.4$; the equivalent depth for identifying candidates in a blank-field submm survey would be closer to $I \sim 23.5$ (Fig. 8), stretching the capabilities of even the largest telescopes. Importantly, however, Barger et al.’s survey allows us to identify candidate counterparts containing AGN based on their spectral properties, and thus allows an upper limit to be imposed on the proportion of submm galaxies which host unobscured and partially obscured AGN. One route to rule out candidate optical counterparts for SCUBA sources is to compare their optical spectroscopic redshifts with redshift limits obtained from their radio and submm properties.

4.6.3 Submm colours

In the absence of bright optical counterparts for most submm sources, and doubts over the applicability of standard optical photometric methods for these dusty systems, we must resort to other redshift indicators. Proposed techniques to estimate redshifts for faint submm galaxies come

from the analysis of their long wavelength SEDs. For example, as discussed by Hughes et al. (1998), the ratio of 450- and 850- μm fluxes, i.e. the spectral shape of dust emission in the rest-frame far-IR, can be used as a crude redshift indicator.

The analysis of the information provided by the 450- μm non-detections of the five 850- μm sources in the HDF (Hughes et al. 1998) suggested that the galaxies all lie at $z > 1$. A similar constraint comes from assuming that the same population of sources are being detected at 450 and 850 μm , and then determining the flux density ratio between the two wavelengths at a fixed source surface density. That the redshift distributions of submm sources at the two wavelengths are likely to be rather similar is supported by Eales et al. (1999) and Blain et al. (1999b). The 450- μm counts are 1000 deg^{-2} brighter than at a flux density limit of 20 mJy. At 850 μm , this surface density is reached at a flux density of about 6.5 mJy. Thus the typical ratio $S_{450}/S_{850} \simeq 3$, suggesting that $\langle z \rangle \sim 3$ if the dust temperature in the population is about 40 K, see Fig. 1. This flux ratio is consistent with the mean value 3.4 ± 0.6 for the five galaxies detected at both wavelengths (see Table 2).

A more reliable estimate of the redshifts of individual sources comes from fitting template SEDs to the entire far-IR/submm/mm SED, provided that sufficient information is available (see for example Ivison et al. 2000a; Frayer et al. 2000; Smail et al. 1999a; Fox et al. 2001). We list the crude redshift ranges derived from this technique in Table 5. However, it is vital to recognise that these estimated redshifts depend strongly on the SED template that is assumed. Because the dust spectrum is thermal, there is a strong degeneracy in the results between the detection of a cooler source at low redshift and a hotter source at a greater distance.

4.6.4 Radio-submm spectral index

A method has been developed recently to estimate redshifts for submm sources exploiting measurements of the 850 μm to 1.4 GHz spectral index, $\alpha_{1.4}^{850}$ (Carilli & Yun 1999, 2000; Blain 1999; Dunne, Clements & Eales 2000; Barger, Cowie & Richards 2000). This technique relies upon the tight correlation between the strength of the far-IR emission (reprocessed UV/optical radiation from massive stars) and radio emission (synchrotron emission from electrons accelerated in supernovae from massive stars) observed in local star-forming galaxies (Condon 1992).

The decline in emission from dust at longer wavelengths is eventually overtaken by the rising synchrotron emission to produce an upturn between the submm and radio wavebands at around 3 mm. This spectral feature is also observed in both high-redshift AGN and star-forming galaxies (see Fig. 10). As proposed by Carilli & Yun (1999), the spectral index observed across this break can be used to provide a crude redshift estimate, with a larger spectral index indicating a higher redshift. The spectral index has the useful property that contamination by radio emission from an obscured radio-loud AGN will tend to reduce the value of $\alpha_{1.4}^{850}$, and thus lead to an underestimate of the redshift. Carilli & Yun (1999, 2000) were able to show that the redshift predictions from $\alpha_{1.4}^{850}$ based on local template spectra and model SEDs were in good agreement with the observed redshifts for a small sample of distant submm sources. Thus $\alpha_{1.4}^{850}$ can

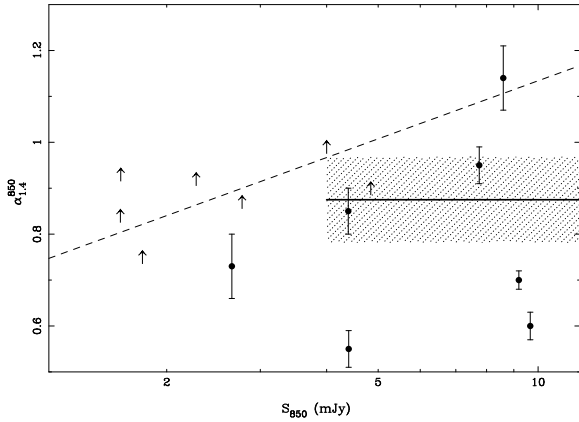


Figure 7. The distribution of radio–submm spectral indices, $\alpha_{1.4}^{850}$, with apparent 850- μm flux for the submm population. The dashed line indicates the approximate source-plane limits of our VLA 1.4-GHz maps. The solid line and hatched region shows the median value and 1- σ confidence limits for the $S_{850} \geq 4$ mJy population. The 850- μm fluxes and limits have been corrected for lens amplification using the estimated amplification factors from Table 4.

be used to place robust *lower* limits on the redshifts of the submm population.

Using the deep VLA 1.4-GHz maps of the seven clusters in our survey (Table 1), Smail et al. (2000) identified radio counterparts to around half of the submm sources, with useful limits on the remainder. They employed models describing the behaviour of $\alpha_{1.4}^{850}$ with redshift from Carilli & Yun (1999) and Blain (1999) to convert their $\alpha_{1.4}^{850}$ measurements and limits into redshift ranges for the galaxies. Using the updated models from Carilli & Yun (2000), which include a representation of the scatter expected in $\alpha_{1.4}^{850}$ as a function of redshift, we estimate the redshift limits and ranges, z_α , for the individual submm galaxies and list these in Table 5.

Taking the various estimates of submm source redshifts listed in Table 5 we can place a crude limit on the median redshift of a complete sample of the submm galaxy population. We include both the reliable and possible spectroscopic redshifts, distribute those galaxies for which upper limits are available on z_α from the radio–submm spectral indices uniformly across their allowed redshift ranges, and place the remaining galaxies with only lower limits on z_α at the minimum allowed redshift (Table 5). In this way we estimate a conservative lower limit of $\langle z \rangle = 2.3_{-1.1}^{+0.8}$ (68 per cent confidence limits) to the median redshift of the submm population brighter than 1 mJy, with only a modest fraction of the submm population at $z < 1$. If we instead adopt a less conservative, more realistic, approach and uniformly distribute those galaxies with only lower limits to z_α across a redshift range from z_α out to some maximum redshift ($z \sim 6$), we obtain a slightly higher median redshift $\langle z \rangle \sim 2.6_{-1.4}^{+1.9}$ (see Hughes et al. 1998; Fox et al. 2001). At these redshifts and submm fluxes, all of the galaxies in our sample must be either ultraluminous or hyperluminous infrared galaxies, $L_{\text{FIR}} \sim 10^{12} - 10^{13} L_\odot$.

In Figure 7 we illustrate the variation of radio–submm spectral index with submm flux for the galaxies in our sam-

ple. The flat flux–redshift relation for submm galaxies shown in Fig. 1 means that any correlation between the redshift-dependent spectral index and 850- μm flux must arise from intrinsic differences in the submm population as a function of luminosity. As pointed out by Smail et al. (2000), there is a hint that the submm galaxies at lower fluxes have typically fainter radio counterparts and thus higher $\alpha_{1.4}^{850}$ values. However, this is at the limits of the sensitivity of even the very deep radio maps used in our analysis. We discuss the variation of the properties of the submm galaxies with their submm flux, as well as the sensitivity of our conclusions on the median redshift of the population to the detailed properties of the submm galaxies, in §6.2.

5 THE PROPERTIES OF INDIVIDUAL SUBMM GALAXIES

In the following we give a brief summary of the properties of the galaxies in our sample:

SMM J02399–0136 – This was the first high-redshift submm galaxy to be detected using SCUBA and remains one of the brightest (850- μm flux of 23 mJy based on a weighted mean of photometry and map measurements, Ivison et al. 1998a). It was quickly identified with a luminous interacting/merging galaxy, L1/L2 at $z = 2.80$, with a far-IR luminosity of $\sim 10^{13} L_\odot$. Both components are resolved in our UKIRT *K*-band image with FWHM of $\sim 0.3\text{--}0.4''$. This system is a relatively bright mid-IR source seen by *ISOCAM* (the flux densities have been revised to 0.13 ± 0.06 and 0.47 ± 0.05 mJy at 7 and 15 μm since those quoted by Ivison et al. 1998a – Metcalfe et al. 2001, in prep). The two components are each resolved by a 1.3'' synthesised beam at 1.4 GHz and appear to have different radio spectral indices (Ivison et al. 1999). The rest-frame UV spectrum exhibits high-ionisation lines with widths of $\sim 1000 \text{ km s}^{-1}$ leading to its classification as a Seyfert-2 galaxy (see also Vernet & Cimatti 2001). However, the strong CO detection of this galaxy suggests that around half of its luminosity arises from a starburst, with the remaining half coming from the AGN (Frayser et al. 1998). Moreover, these observations demonstrate the massive and relatively unevolved nature of this galaxy, with a large gas fraction, an SFR of $\sim 10^3 M_\odot \text{ yr}^{-1}$ and an estimated gas reservoir amounting to $M(\text{H}_2) \sim 2 \times 10^{11} M_\odot$ (this would probably be revised upwards were CO(1 \rightarrow 0) data available – see Papadopoulos et al. 2001). With this SFR, the galaxy could add another $10^{11} M_\odot$ of stars in the next 100 Myr to its already considerable stellar luminosity, $L_V \sim 6L^*$. We note that the recent detection of this galaxy in hard X-rays by *Chandra* confirms the presence of a partially obscured AGN in this source and also supports the claim for a significant starburst contribution to the total luminosity (Bautz et al. 2000).

SMM J00266+1708 – Frayer et al. (2000) present the identification of this submm source with the galaxy M11 based upon 1-mm data from the OVRO Millimeter Array interferometer. A faint near-IR counterpart was identified in their deep Keck *K*-band imaging (we list the properties of this galaxy from their observations in Table 4). The current limits on the *I*-band magnitude of this galaxy do not allow us to classify it as an ERO, but clearly it is very faint and red and so this classification is relatively academic. Based on

the long-wavelength SED of this source, Frayer et al. (2000) suggest its redshift $z \sim 3.5$ and that $L_{\text{FIR}} \sim 10^{13} L_{\odot}$.

SMM J09429+4658 – This source was originally identified with the bright spiral, H1 (Smail et al. 1998). However, near-IR imaging of this field turned up the counterpart H5, one of two bright EROs identified in our UKIRT *K*-band survey. This galaxy is well resolved in the *K*-band image with a seeing-corrected FWHM of $0.5 \pm 0.1''$. This source is discussed in more length in Smail et al. (1999a) who estimate a redshift of $z \sim 2.5$ for this ULIRG ($L_{\text{FIR}} \sim 2 \times 10^{13} L_{\odot}$).

SMM J14009+0252 – The counterpart (J5) to this submm source is extremely faint in the near-IR (and even fainter in the optical). However, there is relatively bright radio emission associated with this galaxy (Table 5), unresolved in a sensitive $1.5''$ -resolution VLA map of the field, and the accurate position allowed us to pinpoint the position of the submm galaxy with sufficient accuracy to warrant a deeper near-IR observation. A near-IR counterpart was eventually detected with $K \sim 21.0$ (Ivison et al. 2000a) although it remains undetected in a very recent *HST* WFPC2 F702W exposure, indicating it has $(R - K) > 5.6$ (Table 4) and therefore classes as an ERO. Balancing the high redshift suggested by the S_{450}/S_{850} flux ratio and the low redshift given by the $\alpha_{1.4}^{840}$ estimator, Ivison et al. (2000a) suggest that this source lies at $z \sim 4$ and class the galaxy as a hyper-luminous IR galaxy, $> 10^{13} L_{\odot}$ with a probable AGN-based contribution to its radio emission.

SMM J14011+0252 – Ivison et al. (2000a) present detailed observations of this submm source, which is identified with a $z = 2.56$ interacting/merging pair of galaxies, J1/J2, with a far-IR luminosity of $L_{\text{FIR}} \sim 6 \times 10^{12} L_{\odot}$. Both optical components are resolved at *K*, J1 being larger ($1.05 \pm 0.05''$) than J2 ($0.4 \pm 0.1''$). The optical spectra of these galaxies show no hint of AGN characteristics (Barger et al. 1999a) and the system is undetected in recent hard X-ray observations with *Chandra* (Fabian et al. 2000), supporting the contention that its luminosity is predominantly produced by a intense starburst (Ivison et al. 2000a). The resolution of the 1.4-GHz radio emission from SMM J14011+0252 in our VLA A+B-array observations also suggests that the far-IR emission from this galaxy is powered by a starburst (Ivison et al. 2001b). Based on optical photometry of the galaxy pair, Adelberger & Steidel (2000) noted that J1/J2 also classes as a Lyman-break galaxy (LBG). However, strong colour differences exist within this system and it is not clear that the source of the starburst activity will have colours typical of a LBG. Indeed, the high-resolution study of SMM J14011+0252 by Ivison et al. (2001b) suggests that the starburst region lies outside the optical extent of the system, close to a previously unidentified extremely red component. The CO detection of this galaxy by Frayer et al. (1999), with a relatively narrow linewidth, indicates that it has a large gas reservoir ($M(\text{H}_2) \sim 10^{11} M_{\odot}$) and that the gas fraction is high (see also Ivison et al. 2001b).

SMM J02399-0134 – This submm source is identified with L3, a ring-galaxy at $z = 1.06$ (FWHM in *K*: $0.6 \pm 0.1''$), which is also a relatively bright VLA 1.4-GHz source and an *ISOCAM* 7- and 15- μm source (with a 15- μm flux density revised to 1.4 ± 0.1 mJy since that quoted by Soucail et al. 1999 — Metcalfe et al. in prep). Optical spectroscopy (and analysis of the mid-IR colours) shows that the galaxy is a Seyfert 1.5–2, and the presence of an obscured AGN was

recently confirmed through a detection in the hard X-ray band by *Chandra* (Bautz et al. 2000). The lensing-corrected far-IR luminosity of this source is $L_{\text{FIR}} \sim 6.5 \times 10^{12} L_{\odot}$. More information about this galaxy is provided by Soucail et al. (1999) and Kneib et al. (2002).

SMM J22471-0206 – There are several possible candidate counterparts to this submm source (Fig. 6), at least two of which (P1 and P4) exhibit sufficiently unusual morphologies to be worthy of further consideration. The morphologies of these in the *HST* *I*-band image of this field show P4 has a bright, compact core with an unresolved arc of emission around it, while P1 exhibits a faint, ‘tadpole’-like tail (Fig. 6). Barger et al. (1999a) obtained optical spectroscopy of both of these galaxies and conclude that P4 has $z = 1.16$ and shows weak AGN characteristics (broad $\text{Mg II } \lambda 2800$ emission), while P1 ($K = 20.1$, $(I - K) = 3.0$) has a featureless spectrum and probably lies at $z \sim 2$. The relatively red colours and AGN signatures in P4 suggest that it is likely to be the correct counterpart, although the low redshift of this galaxy compared to the radio-submm spectral index estimates (Table 5) does raise some doubts.

SMM J02400-0134 – This source was classified as a ‘blank field’ by Smail et al. (1998) and that classification still stands. This is the brightest submm source in the sample without a reliable counterpart, but given the depth of the available near-IR data and the properties of some of the confirmed counterparts to brighter submm sources, this is not particularly surprising (Table 4). Deeper near-IR observations of this region are required to identify any possible counterpart to this source. We note that there are no obvious counterparts in either the *ISOCAM* 15- μm map (Metcalfe et al. 1999; Biviano et al. 2000) or the *Chandra* hard X-ray image of this field (Bautz et al. 2000) which both argue for a high redshift on *K*-correction grounds.

SMM J04431+0210 – The near-IR counterpart, N4, to this source is one of the EROs identified in the sample (Smail et al. 1999a). This galaxy lies very close to an edge-on spiral member of the foreground cluster lens, which was the identification originally proposed by Smail et al. (1998). Its extreme optical-IR colour mean that it is invisible on deep *HST* and Keck optical images of this field, although it is well-detected in the *K*-band with an estimated FWHM of $0.4 \pm 0.1''$ after correcting for lens amplification. Smail et al. (1999a) discuss various redshift constraints for this source and suggest that it probably lies at $z \sim 3 \pm 0.5$ and has $L_{\text{FIR}} \sim 5 \times 10^{12} L_{\odot}$. There is a small additional contribution to the amplification of this source caused by the proximity of the foreground spiral galaxy.

The following sources are the fainter half of our sample, with intrinsic fluxes of $\lesssim 4$ mJy. Our follow-up of these sources has not been as extensive as the studies of the brighter sources discussed above, and so the information available is more limited and our discussion is necessarily more speculative.

SMM J21536+1742 – There are several optically faint candidate counterparts in the vicinity of this submm source. Barger et al. (1999a) obtained spectroscopy of two: K2, for which they suggest a possible redshift of $z = 1.60$ from a low signal-to-noise spectrum; and K3, an absorption-line galaxy at $z = 1.02$ which appears to be weakly detected in the *ISOCAM* 15- μm image of this field at a flux of ~ 0.2 mJy (Lémonon et al. 1998). K3 has $K \sim 18.5$ and

$(I - K) = 4.7 \pm 0.1$, excluding the northern end of the galaxy which is apparently blended with a blue point source – the effect of this blend on the spectroscopic observations is unknown. The colours of K3 are too red for a passive stellar population at $z \sim 1$ and suggest that dust plays a role in its apparent properties, in agreement with its detection at $15 \mu\text{m}$. Given the unusual properties of K3 we suggest that it may contribute to the submm emission in this region, perhaps confusing an optically fainter submm source closer to the position of K2. The reduced sensitivity of the 1.4-GHz map of this field (due to the bright central galaxy) hinders the resolution of this question.

SMM J00265+1710 – The bright galaxies to the south of this source (M6 in Fig. 6) are in the foreground of the cluster at $z = 0.21$ (Barger et al. 1999a) and, apart from these, no additional spectroscopy is available. Smail et al. (2000) identify a radio source outside of the nominal submm error box which could be the counterpart. This radio emission may be associated with the faint, extended galaxy to the north-east which has $K = 19.7 \pm 0.2$ and $(I - K) = 2.8 \pm 0.2$. We note that $15\text{-}\mu\text{m}$ observations were taken of this field with *ISOCAM*, which may help in disentangling the identification of this source.

SMM J22472–0206 – There are several faint galaxies in the vicinity of this submm source. Barger et al. (1999a) suggested a possible redshift of $z = 2.11$ for P2, consistent with the non-detection of this submm source at 1.4 GHz. To the south, P6 is relatively faint and blue ($I = 24.5$, $(I - K) < 2.8$), and a very faint and apparently very red galaxy (P7 in Fig. 6) is just visible to the south of an $I \sim 24$ galaxy east of P2. P7 is only just detected in our UKIRT K -band image, but it appears to be an ERO with $K = 20.7 \pm 0.3$ and $(I - K) > 5$. Again this field is a candidate for a confused source arising from a blend of two submm sources associated with P2 and possibly P7.

SMM J00266+1710 – Another apparently blank field. The proximity of the arclet, M3, to this source led Smail et al. (1998) to suggest this was a possible counterpart. However, the comparison of the arclet’s redshift, $z = 0.94$ (Barger et al. 1999a) and the redshift estimate from the $\alpha_{1.4}^{850}$ limit, $z > 1.9$, suggests that this interpretation is incorrect, and the true counterpart must therefore be significantly fainter; we therefore classify this as a probable blank field. Nevertheless, the highly distorted morphology of the arclet, produced by the gravitational lens, gives a graphic illustration of the likely amplification suffered by this submm source. Indeed, if the source redshift is significantly greater than $z \sim 1$ it is probable that this source actually comprises a blend of the brightest two images of a multiply-imaged submm galaxy. The third image would be below the detection threshold of our SCUBA map.

SMM J00267+1709 – This field is classified as blank in the analyses of Smail et al. (1998) and Barger et al. (1999a). Our relatively shallow UKIRT K -band image has not revealed any galaxies with $K < 20.6$ which are undetected in the *HST* I -band image (Fig. 6) and so our classification for this source remains as a blank field.

SMM J04433+0210 – This submm source has the lowest apparent flux of any of the sources in our catalogue and unfortunately falls outside the archival *WFPC2* F702W exposure of this field (Smail et al. 1998). Optical imaging covering this source was only acquired after the spectroscopic

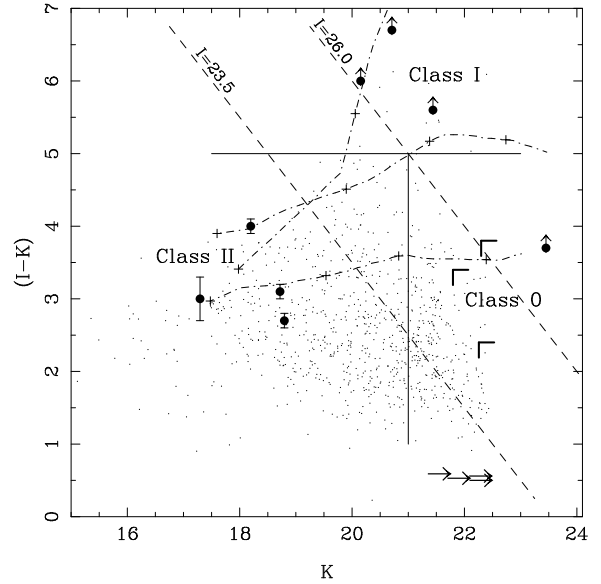


Figure 8. The distribution of proposed and confirmed counterparts to the submm sources on the $(I - K)$ – K colour-magnitude plane. Sources with possible counterparts which are only detected in the optical passbands are marked with \square . Sources with no counterparts in K or I are plotted in the lower-right corner and we assume the same $(I - K)$ limit as that measured in $(R - K)$ for SMM J14009+0252. The apparent magnitudes have been corrected assuming the lens amplifications listed in Table 4. We also plot, for comparison, the distribution of a deep K -selected field sample as small points (L. Cowie, priv. comm.) and we show the rough boundaries of the classification scheme for counterparts to submm sources proposed by Ivison et al. (2000b). The dashed lines show the approximate I -band magnitudes limits (corrected for lens amplification) for spectroscopic identification on a 10-m telescope and deep imaging with a ground-based 10-m or *HST*. The three dot-dashed lines show the colour tracks expected for ULIRGs with $M_K = M_K^* + 2$ and the optical-UV SEDs measured by Trentham et al. (1999). These tracks start at $z = 1$ (at $K \sim 18$) and tick marks show increments of $\Delta z = 1$.

survey of Barger et al. (1999a) was completed. There appears to be a relatively bright candidate optical and radio counterpart to this submm source, N5.

The following two submm sources are both identified with the central galaxies in the lensing clusters used in our survey:

SMM J21536+1741 – This source corresponds with the central galaxy in the lensing cluster A 2390 ($z = 0.23$).

SMM J14010+0252 – This source has also been identified with the central galaxy in the cluster lens A 1835 at $z = 0.25$. Unlike SMM J21536+1741, this galaxy appears to be undergoing significant star-formation activity (see Edge et al. 1999 for a more detailed discussion of both central galaxies).

6 THE PROPERTIES OF THE SUBMM POPULATION

We begin our discussion of the nature of the submm population by focusing on the properties of these galaxies as out-

lined in the previous sections. We start with those observables which are available for the whole sample, such as the characteristics of their SEDs, before turning to more detailed information which only exists for a subset of the sample. As the detailed follow-up work has concentrated on the brighter sources in our survey (e.g. Frayer et al. 2000), we will rely on their properties when discussing the detailed characteristics of the submm population, bringing in the fainter sources where there are suggestions of differences in their behaviour.

6.1 Optical and near-infrared properties

The discussion in §5 of the optical and near-IR counterparts to the individual submm sources highlighted the wide range in the properties of submm galaxies at these wavelengths: although the sources span less than an order of magnitude in their submm fluxes, their counterparts span three orders of magnitude in their optical fluxes. In an attempt to identify some structure in this variety, Ivison et al. (2000b) suggested a phenomenological classification scheme for the counterparts to submm sources, analogous to that used for protostars (Adams et al. 1987). They defined three broad classes related to the observational properties of likely counterparts using operational definitions based upon the typical depths achieved in follow-up observations ($I \sim 26$, $K \sim 21$, Fig. 8). This magnitude limit in the near-IR corresponds roughly to an unobscured L^* galaxy at $z > 2-2.5$, whereas the effective dividing line in colour, $(I-K) > 5$, usefully separates the colours expected from unreddened stellar populations at $z \lesssim 6$ from those exhibited by dusty galaxies (Pozzetti & Mannucci 2000). This classification scheme therefore provides a crude differentiation between counterparts where dust is likely to play a significant role in the optical/IR colours and luminosity of the galaxy from those where it does not.

In the Ivison et al. scheme, Class-0 objects are faint in both optical and near-IR passband, with $K \gtrsim 21$ and $I \gtrsim 26$; these are likely to be either highly obscured or very high-redshift galaxies (here we also include those sources which are sufficiently faint in the optical that they cannot be spectroscopically identified, $I \gtrsim 23.5$). Class-I sources have counterparts in the near-IR brighter than $K \sim 21$, but not in the optical ($I > 26$) and hence will be EROs. Finally, Class-II sources have obvious optical and near-IR counterparts. When spectroscopic information is available for Classes I and II, they can be further subdivided into the three spectroscopic types used to classify local ULIRGs (e.g. Sanders et al. 1988): *a*, pure starburst; *b*, type-II AGN, narrow-line but high excitation spectra such as Seyfert 2; and *c*, type-I AGN, e.g. classical broad-line AGN such as Seyfert 1. Class II submm sources may overlap with the most strongly star-forming and massive LBGs and QSOs.

We plot the possible counterparts to the 15 submm sources discussed in §5 on the $(I-K)-K$ colour-magnitude plane in Fig. 8 and overplot the classification boundaries. We also show the colour-magnitude redshift tracks expected for luminous galaxies with UV/optical SEDs similar to the three ULIRGs studied by Trentham et al. (1999). These illustrate the wide variation in rest-frame UV/optical obscuration encountered in this population locally.

We find that our sample consists of 8–9 Class-0 counterparts (60 per cent), 2–3 in Class I (15 per cent) and 4

(25 per cent) in Class II, depending upon the exact boundaries adopted. It is clear that the majority of the submm sources are extremely faint in optical wavebands and will thus be difficult to detect in optical surveys for high-redshift star-forming galaxies. The four Class-II galaxies for which there are detailed spectroscopic observations can be further sub-divided into one Class-IIa star-forming galaxy and three Class-IIb obscured AGN. Although many of the submm sources with optical counterparts exhibit some level of AGN activity, the presence of strong stellar absorption features in their optical spectra indicate that the non-thermal emission does not dominate in the optical/near-IR wavebands.

Comparing the colours and magnitudes of the submm sources with the tracks from Trentham et al. (1999) in Fig. 8, we see that the four Class-II galaxies have colours and brightnesses consistent with those expected for $\gg L^*$ galaxies with ULIRG-like UV/optical SEDs at $z \sim 1-3$. The 2–3 Class-I sources have colours similar to the reddest of the local ULIRGs placed at $z \gtrsim 2$, with apparent magnitudes suggesting that they too have extreme rest-frame optical luminosities, $\sim 5L_K^*$ (much higher than seen in similar local systems, Trentham priv. comm.). Clearly, the luminous submm galaxies in both of these classes have already built up considerable stellar populations. Finally, even the relatively blue colours of some of the optical sources within the Class 0 error boxes are still consistent with the colours of the bluest local ULIRGs, and so cannot be ruled out as possible counterparts to the submm sources without further information.

Figure 9a displays the K -band magnitudes or limits for the submm galaxies, as a function of their apparent 850- μm fluxes (both corrected for lens amplification). As expected, the very different behaviour of the K -correction in these two wavebands results in little correlation between the brightness of galaxies in the submm and near-IR wavebands, with the brightest submm galaxies in our sample spanning a range of 6 mag. ($250\times$) in the K band. Nevertheless, it does appear that bright near-IR counterparts are not seen for the faintest submm galaxies, with $S_{850} \lesssim 4$ mJy, which typically show only very faint K -band counterparts (the majority simply being upper limits). This may reflect real differences in the mix of classes seen at high and low far-IR luminosities, or alternatively could simply result from the small sample size. Either way, the possibility of a difference between the bright and faint submm galaxies undermines attempts to extrapolate the properties of the most luminous submm sources to the fainter sources which dominate the far-IR extragalactic background (FIRB).

We conclude this section by briefly discussing the near-IR (rest-frame optical) morphologies of the Class-I and II sources (Fig. 6; see also Ivison et al. 1998a, 2000a and Smail et al. 1999a). Where the available imaging has sufficient signal to noise we find that all of the sources have extended rest-frame optical emission (§5), with intrinsic FWHM of 0.5–1'' (or 5–10 kpc at $z \sim 2-3$), with several comprising multiple components (e.g. L1/L2, J1/J2, L3). Concentrating on the multiple-component systems, L1/L2 and J1/J2, we note that the spatial separation of the individual components within these systems is 2–3'', corresponding to ~ 10 kpc in the source plane. Such large separations are claimed to be relatively rare in local ULIRG mergers (Murphy et al. 1996; Solomon et al. 1997; although see Rigopoulou et al.

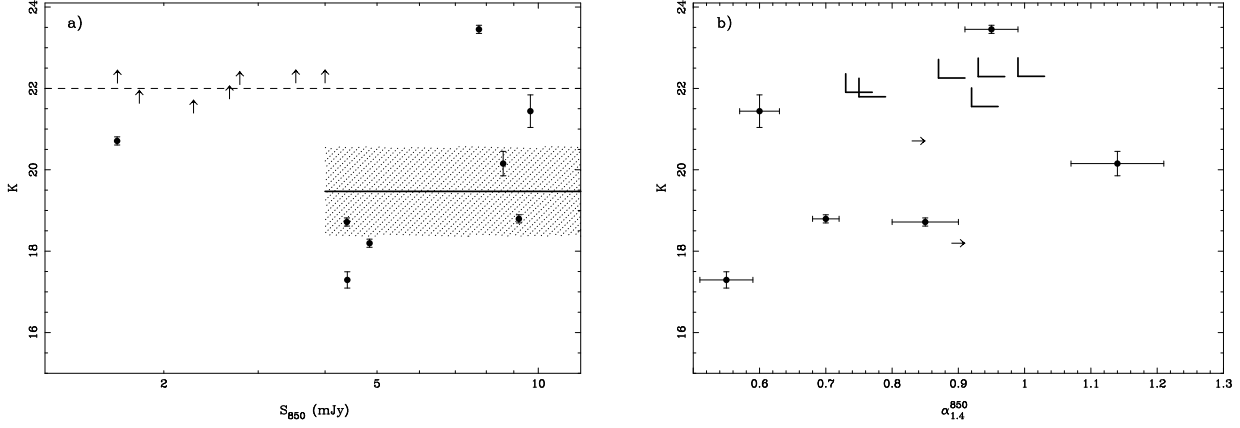


Figure 9. a) The distribution as a function of apparent 850- μm flux of the apparent K -band magnitudes of counterparts for the submm sources. The dashed line indicates the approximate source-plane limits of our UKIRT K -band imaging. The solid line and hatched region shows the median value and 1- σ confidence limits for the $S_{850} \geq 4 \text{ mJy}$ population. Note the very wide range in K -band magnitude exhibited by the brightest submm sources, $S_{850} \gtrsim 4 \text{ mJy}$, whereas the faintest submm sources do not typically possess bright K -band counterparts. b) The distribution of the K -band magnitude of the counterparts against radio-submm spectral index, $\alpha_{1.4}^{850}$. There appears to be a weak trend for fainter counterparts to have higher $\alpha_{1.4}^{850}$ values, although the scatter is considerable. The 850 μm flux and K -band magnitudes in both panels are corrected for lens amplification using the values given in Table 4.

1999) and may suggest that ULIRG phase occurs at a much earlier stage of mergers at high redshift, either because of their higher gas fractions or due to other factors which lower the stability of their gas reservoirs (e.g. the absence of a strong bulge component, Mihos & Hernquist 1996; Bekki et al. 1999). A deeper survey of the restframe optical morphologies of the complete sample must await the revival of *NICMOS* on-board *HST*.

6.2 Submm, far-IR and radio properties

The submm galaxies for which we have good information on their rest-frame SEDs are naturally those with reliable redshifts. We show in Fig. 10 the SEDs for SMM J02399–0136 at $z = 2.80$, SMM J14011+0252 at $z = 2.56$ and SMM J02399–0134 at $z = 1.06$, covering the rest-frame wavelength region from the near-IR to the radio. The spectroscopic observations show that SMM J02399–0136 and SMM J02399–0134 both host obscured AGN, while SMM J14011+0252 appears to be a pure starburst (§5). Of the three, SMM J02399–0136 is the most luminous, but the other two systems have comparable bolometric luminosities. However, irrespective of their different optical spectra and luminosities, Fig. 10 shows that these three submm-selected galaxies have very similar far-IR SEDs. The only significant difference occurs in the radio waveband, at rest-frame frequencies about 4 GHz, where the three radio-quiet galaxies differ by a factor of ~ 5 in flux density. The brightest is SMM J02399–0136, followed by SMM J02399–0134 and then SMM J14011+0252. We interpret this sequence as arising from an increasing contribution from an active nucleus going from the pure starburst (SMM J14011+0252) to a luminous type-2 AGN in SMM J02399–0136. Apart from a weak contribution in the radio, this change makes little overall difference to the radio-far-IR SEDs of the galaxies, however it does illustrate the degree of uncertainty which should be expected when trying to use the radio-submm spectral

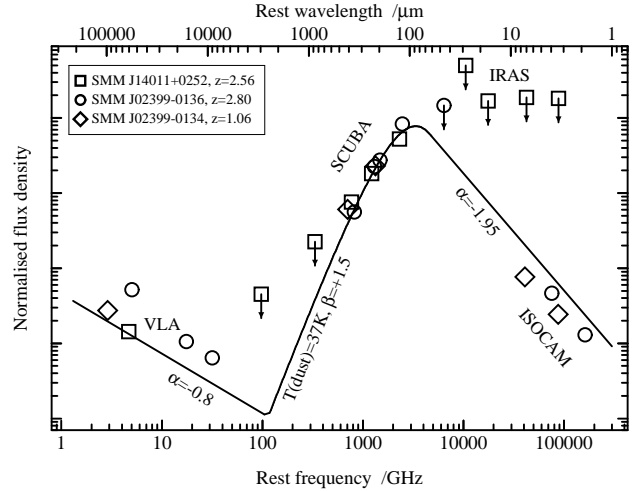


Figure 10. The rest-frame SEDs for the three submm galaxies in our survey with reliable spectroscopic redshifts: SMM J02399–0136 (L1/L2), SMM J14011+0252 (J1/J2) and SMM J02399–0134 (L3), normalised in flux density at a rest-frame wavelength of 250 μm . We overplot the best-fit SED used to model the FIRB and counts, as discussed in §6.5: a greybody with $T_d = 37 \text{ K}$, $\beta = +1.5$, with power-laws of index $\alpha = -1.95$ (where $F_\nu \propto \nu^{+\alpha}$) beyond 60 μm , and $\alpha = -0.80$ from 1.4 GHz to 3 mm.

index as a redshift estimator for galaxies hosting radio-loud AGN. The range in rest-frame radio power shown by the three galaxies compared here would result in a systematic reduction of the spectral index by $\delta\alpha_{1.4}^{850} = -0.3$, and an equivalent reduction in the estimated redshift of the source.

At the shorter wavelengths covered by Fig. 10, we see that the SEDs are poorly constrained between 10–100 μm in the rest frame, a situation that should soon be resolved by *SOFIA* and *SIRTF*. At the slightly longer wavelengths observed by *SCUBA*, we find the average SED of the three

galaxies is consistent with the characteristic spectral index $\alpha \simeq 3.5 \pm 0.5$, of optically-thin emission from dust grains. Simple fits to this composite SED cannot, of course, accurately constrain the dust temperature, although the data for all three galaxies are consistent with the T_d range of 35–50 K found for other dusty, high-redshift systems (Benford et al. 1999). Higher temperatures can only be fitted if the opacity of the dust becomes significant at wavelengths of about 100–200 μm .

As mentioned in §4.6, the redshifts estimated from the spectral index are sensitive to the assumed temperature of the dust, T_d , in the submm galaxies (Blain 1999) and so reducing T_d would allow a lower median redshift for the population. However, only if we force the entire submm population to have a characteristic dust temperature less than 30 K can we start to push the median redshift much below $\langle z \rangle \sim 2$. There is no evidence for such a cold characteristic temperature in any of the brighter submm galaxies with confirmed identifications and redshifts, nor is there any physical reason to expect that dust in high-redshift starbursts should be any cooler than that in local LIRGs and ULIRGs.

Looking at the population as a whole, if typical submm-selected galaxies have cool dust temperatures (and thus lay at low redshifts), for example an analogue of the Milky Way with ~ 17 K (Reach et al. 1995), they would be detectable at the mJy level using SCUBA and at the μJy level using the VLA, consistent with the observations. However, their optical counterparts would be very bright in *HST* and ground-based follow-up images. Based on the data presented here, such sources can only represent a few per cent of SCUBA-selected galaxies.

Is there any evidence for differences in dust temperature within the submm population? Fig. 9b illustrates the variation in amplification-corrected apparent *K*-band magnitude with radio-submm spectral index of the source. There may be a weak tendency for sources with higher $\alpha_{1.4}^{850}$ indices to have fainter counterparts, but any trend is weakened by the large scatter, a factor of 100 at a fixed $\alpha_{1.4}^{850}$. This large scatter may reflect both the crudeness of $\alpha_{1.4}^{850}$ as a redshift indicator and the strong variation in the rest-frame UV/optical obscuration in the submm population.

Higher values of $\alpha_{1.4}^{850}$ are expected to correspond to galaxies with either higher redshifts for the same SED, or to cooler dust temperatures for the same redshift (Blain 1999). The observations are consistent with either explanation. If the redshift distribution is systematically higher for fainter sources – a straightforward explanation, and one that is hinted at in Fig. 9b – then it will be difficult to test this idea, as the brightness of the counterpart to the submm source will be reduced in all other wavebands. The distribution of the *K*-band counterparts in Fig. 9a suggests that the fainter submm sources may indeed have fainter near-IR counterparts, which would support this suggestion, although this could simply indicate that the fainter sources are more obscured. Alternatively, if the fainter sources are systematically cooler, then the bolometric luminosity derived for them, as associated with a given 850- μm flux density, will be much less as compared with that estimated using a hotter dust temperature, and so their counterparts in other wavebands would also be expected to be systematically fainter; however, the typically lower redshift of the counterparts might make their detection in the *K*-band easier in this

case. The resolution of this issue awaits both accurate multi-band photometry of submm-selected galaxies using *SIRTF* and *SOFIA* at wavelengths corresponding to the rest-frame peak of their SED, and the measurement of redshifts for submm galaxies over a wider range of flux density.

Using the new estimates for the redshifts and limits from §4.6.4, listed in Table 5, we conclude that at least half of the submm population down to a median *intrinsic* 850- μm flux of ~ 3 –4 mJy have redshifts above $z = 2$. This result is consistent with the expectations from the 450-/850- μm flux ratios discussed in §4.6.3.

If the median redshift of the submm population is $z > 2$ and we adopt a mid-IR SED for the galaxies similar to Arp 220 then their predicted 15- μm fluxes would typically be $< 10 \mu\text{Jy}$ – well below the *ISOCAM* detection limit. The relatively high rate of *ISOCAM* 15- μm detections we find therefore suggests that Arp 220 is not a good prototype for the mid-IR SED of a faint submm galaxy, which are typically brighter at mid-IR wavelengths. Fig. 11 illustrates the mid-IR–submm spectral indices of the current sample of galaxies with both *SCUBA* and *ISO* observations (or limits) along with the behaviour expected from a number of SEDs. The observations appear to rule out Arp 220-like SEDs in the mid-IR (which are too red), but are well described by model SEDs of less optically-thick starbursts (Dale et al. 2001; Eales et al. 2000). Fig. 11 also illustrates the behaviour of the mid-IR–submm spectral index from the composite SED used by Blain et al. (1999b) to model the FIRB and counts (see §7), including the faint counts of galaxies detected by *ISOCAM* at 15 μm and the deep counts of radio galaxies determined at frequencies of 1.4 and 8.4 GHz using the VLA (see §6.5). This SED has $T_d = 37$ K, $\beta = +1.5$ and a mid-IR spectral index of -1.95 , and lies on the low-redshift far-IR–radio correlation. It clearly provides an adequate representation of the behaviour of individual galaxies in the mid-IR waveband.

6.3 Dynamical, gas and dust masses

Dynamical information is available for three galaxies in our sample: SMM J02399–0136 (Frayser et al. 1998); SMM J14011+0252 (Frayser et al. 1999; Ivison et al. 2001b) and SMM J02399–0134 (Kneib et al. 2002). This comes from mapping redshifted CO line emission in these galaxies with the OVRO and IRAM interferometers. The width of the molecular line provides an estimate of the dynamical mass of the system, while the strength of the line can be used to estimate the total molecular gas mass of the systems, assuming a conversion from CO gas mass to total molecular gas mass (mostly H_2), an assumption which may be uncertain at the factor of $\gtrsim 4$ level (Downes & Solomon 1998; Papadopoulos et al. 2001).

It is interesting to note that although SMM J02399–0136 and SMM J14011+0252 have very different optical classifications, they have very similar (and high) far-IR to CO ratios: $L_{\text{FIR}}/L'_{\text{CO}} \sim 500 L_{\odot} \text{K}^{-1} \text{km s}^{-1} \text{pc}^{-2}$, at the high end of the values seen in local ULIRGs (Solomon et al. 1997). This suggests that their prodigious far-IR luminosities are powered by similar physical processes, probably highly efficient star formation (Solomon 2001).

The dynamical masses in the central 10–20 kpc inferred for these systems are 1 – $2 \times 10^{11} \sin^{-2}(i) M_{\odot}$ (where i is the

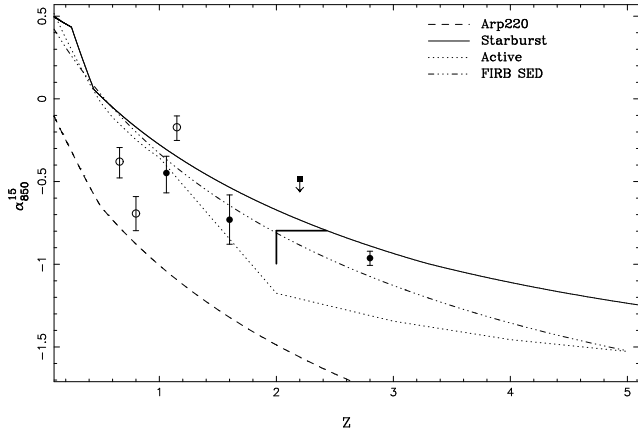


Figure 11. The variation in the spectral index between 15 and $850\ \mu\text{m}$ as a function of redshift for a range of SEDs. We show the expected variation in the spectral index for the SED of Arp220, the starburst SED from Eales et al. (2000), the most active SED from Dale et al. (2001) and the best-fit SED used to fit the mid- and far-IR background from Blain et al. (1999b) (assuming $T_d = 37\ \text{K}$, $\beta = +1.5$ and a mid-IR spectral index, -1.95). We plot the measurements from the SCUBA Lens Survey as filled symbols, the open symbols show joint SCUBA and *ISOCAM* detections from Hughes et al. (1998) and Eales et al. (2000). The upper limit represents the typical limits on the ~ 80 per cent of the submm sources undetected by *ISOCAM* from Eales et al. (2000) and Hughes et al. (1998).

unknown inclination angle), while their total molecular gas masses are estimated at $1\text{--}2 \times 10^{11}\ M_\odot$, assuming a CO luminosity to molecular gas mass conversion factor, $\alpha = 4\ M_\odot\ (\text{K km s}^{-1}\ \text{pc}^2)^{-1}$. This suggests that molecular gas is a dynamically important, and perhaps dominant, constituent in the central $\sim 10\ \text{kpc}$ of these galaxies (see Frayer et al. 1998, 1999). Combining these dynamic mass estimates with the measured rest-frame optical luminosities of these galaxies we find very low mass-to-light ratios: $M_{\text{dyn}}/L_V \sim 0.3$, as expected for star-forming systems dominated by very recent star formation, $\sim 100\ \text{Myrs}$ (Salasnich et al. 2000).

Adopting $k_d = 0.15(\lambda_0/800\ \mu\text{m})^{-1.5}$ for the standard dust emission parameter, where λ_0 is the rest-frame wavelength, in order to compare the results with other distant sources, we estimate dust masses of $M_d = 0.5\text{--}5 \times 10^8\ M_\odot$ for the typical submm galaxies in our sample, based on dust temperatures of $T_d = 40 \pm 10\ \text{K}$ (see §6.2). Given the modest dust yield from a standard IMF, these large dust masses provide further support for the high SFRs claimed for these galaxies, assuming of course that type-II supernovae are a significant source of dust in the early Universe, which has yet to be demonstrated convincingly.

6.4 Power source: AGN versus starburst

The source of the extreme luminosities of the submm galaxy population detected by SCUBA remains a key problem for interpreting their nature and their relevance for models of galaxy formation and evolution. Unfortunately, submm observations alone are unable to discriminate between luminous dusty galaxies powered by massive stars or AGN, although the resolution of a handful of sources in the radio

or millimeter on scales of $\lesssim 5''$ suggests that the submm emission from these galaxies comes from an extended region rather than a central AGN (or in fact nuclear starburst). This result cautions against the use of very high resolution radio or millimeter facilities for surveys to identify this population.

While it is plausible that AGN powered dusty galaxies could on average have hotter dust temperatures, rendering them less likely to be selected in submm surveys (Fig. 1), at present there is insufficient information to confirm this. We therefore have to resort to secondary indicators of AGN activity to determine their prevalence in the submm population as a whole. We stress that even when an AGN is known to be present, determining its contribution to the overall energetics of the submm emission is still far from trivial (e.g. Frayer et al. 1998, 1999).

There are at least three unambiguous examples in our sample of submm galaxies which harbour AGN nuclei: L1/L2, L3 and P4 (Table 5), all based on broad lines visible in optical spectroscopy. In all three cases these AGN show signatures of dust obscuration in their line ratios. For the optically-faint majority of the sample, however, we have to rely on other tracers of AGN activity, the most powerful being hard X-ray emission (Fabian et al. 2000; Bautz et al. 2000; Hornschemeier et al. 2000; Page et al. 2001).

Using the *ROSAT* X-ray limits from §4.5 and our observed submm fluxes for the individual sources, we estimate that the typical submm galaxy has a submm–X-ray spectral index, α_X^S (Fabian et al. 2000), of $\alpha_X^S \gtrsim 1.1$ (assuming a $\Gamma = 2$ power-law for the X-ray emission). We compare the limits on α_X^S for the submm sources with five quasars at $z > 4$ using the combined *ROSAT* X-ray observations of Kaspi et al. (2000) and submm photometry from McMahon et al. (1999). These quasars have $\alpha_X^S \sim 0.9 \pm 0.1$, with the most submm-luminous example being BR 1202–0725 with $\alpha_X^S \sim 1.1$. We conclude that if AGN are present in typical submm galaxies then they are more obscured than the dusty and gas-rich $z = 4.69$ QSO BR 1202–0725 (Omont et al. 1996). To better quantify this statement, we use the obscured AGN models from Fabian et al. (2000) and Gunn & Shanks (2001) and suggest that if AGN are present in the typical submm galaxy then they must lie behind columns of $N(\text{H}) > 10^{23}\ \text{cm}^{-2}$. The more sensitive *Chandra* observations of a smaller sample suggest that if submm galaxies host AGN then these must be Compton-thick ($N(\text{H}) \gg 10^{24}\ \text{cm}^{-2}$) and the amount of unprocessed AGN emission which does escape by scattering must be small (Fabian et al. 2000; Bautz et al. 2000; Hornschemeier et al. 2000; Almaini et al. 2001).

Thus the available information suggests that the fraction of SCUBA galaxies which host optically-identifiable AGN is between 10 and 20 per cent (Barger et al. 1999a) and that if AGN are present in the majority of the submm population then these must be sufficiently obscured that they are unlikely to be visible in the optical anyway. The low fraction of AGN-dominated systems is consistent with much more detailed surveys of similar luminosity ULIRGs at $z \sim 0$, which find 20–30 per cent are AGN-dominated (Genzel et al. 1998).

Better constraints on the proportion of AGN in the submm population await more sensitive hard X-ray observations with *XMM/Newton* (in blank fields) or *Chandra* (Al-

maini et al. 2001), searches for broad emission lines in the less dust-sensitive near-IR wavebands and surveys for hot dust emission from AGN-illuminated tori in the mid-IR.

6.5 Constraining the evolution of dusty galaxies

Finally, we discuss the exploitation of the submm population for understanding the wider issue of the evolution of dusty galaxies. This section revisits the results of Blain et al. (1999b, 1999c) to constrain simple models for the evolution of luminous dusty galaxies and provide some physical insights into the processes driving their activity.

In the local Universe, the luminosity function of luminous dusty galaxies is best constrained at $60\ \mu\text{m}$ based on the *IRAS* survey (Saunders et al. 1990). Additional information about these galaxies is also available at $100\ \mu\text{m}$ (Soifer & Neugebauer 1990). These wavelengths are close to the peak of the SED for any reasonable dust temperature and the ratio of the bright counts at 60 and $100\ \mu\text{m}$ implies a luminosity-averaged dust temperature $T_d \sim 35\text{--}45\ \text{K}$. $850\text{--}1000\ \mu\text{m}$ observations of galaxies detected by *IRAS* (Dunne et al. 2000; Lisenfeld et al. 2000) provide a longer wavelength baseline and hence an excellent probe of the SED. These indicate $T_d = 36 \pm 5\ \text{K}$ and a Rayleigh–Jeans spectral index of 3.3 ± 0.2 (i.e. $\beta = +1.3$, but see Dunne & Eales 2001). The population of low-redshift dusty galaxies can be divided into relatively short-lived warm interacting/starbursting galaxies and long-lived cooler quiescent galaxies (Blain et al. 1999c; Barnard & Blain 2001); however, the details of this distinction are relatively unimportant for studies of high-redshift galaxy evolution. Any low-luminosity, low-temperature dusty galaxies missing from existing surveys do not contribute significantly to the luminosity density, even at low and moderate redshifts (Chapman et al. 2002).

The form of evolution of the baseline low-redshift far-IR luminosity function $\Phi_0(L)$ must be dominated by pure-luminosity evolution, that is $\Phi(L, z) \simeq \Phi_0[L/g(z), 0]$, to ensure that the far-IR background radiation intensity is not exceeded. Number-density evolution is also likely to be involved, but must be dominated by luminosity evolution (Blain et al. 1999b; Chapman et al. 2001c). The evolution function $g(z)$ is determined by demanding that the background radiation intensity, counts and redshift distributions of dusty galaxies are all in agreement with observations. These observations are, in order of increasing redshift, the faintest counts and redshift distributions of $60\text{--}\mu\text{m}$ *IRAS* galaxies, deep 90-- and $170\text{--}\mu\text{m}$ counts from *ISO*, the spectrum of background radiation from *COBE*, and the faint counts and limited redshift information of distant galaxies detected using SCUBA at 450 and $850\ \mu\text{m}$ and MAMBO at $1.2\ \text{mm}$.

Several approaches can be taken to investigate the evolution. The simplest is to assume a parametric form for $g(z)$ and fit this to the data to construct a model which relates observations across a range of wavebands in a simple phenomenological manner (Blain et al. 1999b; see also Rowan-Robinson 2001). This has the advantage of requiring few parameters to model the galaxy SED so that the form of evolution can be well constrained using the sparse observational information. A more physically motivated approach connects the evolving mass function of galaxies to the associated luminosity function using a prescription for both

star formation and the fueling of AGN (Baugh et al. 1998; Guiderdoni et al. 1998; Blain et al. 1999c); however, care must be taken to avoid getting lost in the space of available free parameters. Without an additional population of short-lived, very luminous galaxies, the simplest standard semi-analytical models, which include star formation in the gas that cools in galaxy disks, fail to account for the observed surface density of SCUBA and MAMBO sources (Guiderdoni et al. 1998).

6.5.1 A simple parametric model

This approach was adopted by Blain et al. (1999b), who assumed a local $60\text{--}\mu\text{m}$ luminosity function, an SED defined by a single dust temperature T_d and a form of evolution $g(z) = (1+z)^\gamma$ at low redshifts. T_d and γ are determined from the $60\text{--}\mu\text{m}$ *IRAS* counts and the latest *ISO* counts at 90-- and $175\ \mu\text{m}$ (Juvella et al. 2000). We derive $T_d = 37 \pm 3\ \text{K}$ and $\gamma = 4.05 \pm 0.15$, assuming a Rayleigh–Jeans spectral index of $+3.5$. These results differ only slightly from the original analysis of Blain et al. (1999b), based on more limited *ISO* data, $T_d = 38 \pm 4\ \text{K}$ and $\gamma = 3.9 \pm 0.2$. Equally, changing to the more popular non-zero- Λ cosmology does not significantly alter this result (Blain 2001).

The characteristic dust temperature we derive is consistent with subsequent SCUBA measurements of local luminous *IRAS* galaxies (Dunne et al. 2000), suggesting a continuity in the properties of this population between low and moderate redshifts. The value of γ we find is closer to that claimed for the evolution of the optical luminosity density (Lilly et al. 1996) and mid-IR counts (Xu 2000) than the value of $\gamma = 3$ often assumed to describe the evolution of galaxies in the far-IR waveband.

At higher redshifts, the behaviour is not well constrained by *ISO* observations (although future *SIRTF* surveys will make a major impact in this area) and we rely instead on the form of the background radiation intensity (Fixsen et al. 1998) and the counts of SCUBA galaxies. These are somewhat degenerate, although the SCUBA data provide the better constraint. The most useful of the various simple parametric forms adopted by Blain et al. (1999b) to describe the evolution of Φ at high redshifts is the so-called ‘Gaussian’ model, in which $g(z)$ at moderate and high redshifts is represented by a Gaussian in cosmic epoch. Since then, progress has been made in developing a more appropriate form of $g(z)$, which is fully compatible with models of cosmic chemical evolution and naturally includes a peak in the evolution function (Jameson 1999):

$$g(z) = (1+z)^{3/2} \text{sech}^2[b \ln(1+z) - c] \cosh^2 c. \quad (1)$$

At low redshifts, $\gamma \simeq (3/2) + 2b\sqrt{1 - \text{sech}^2 c}$. Using all available observational data, the results $b = 2.2 \pm 0.1$ and $c = 1.84 \pm 0.1$ are obtained; see the solid line in Fig. 12. These results are similar to those derived by Blain et al. (1999b), but use the more accurate 175-- and $850\text{--}\mu\text{m}$ counts now available, as well as the limits on the probable redshift distribution of the $850\text{--}\mu\text{m}$ population from §4.6.

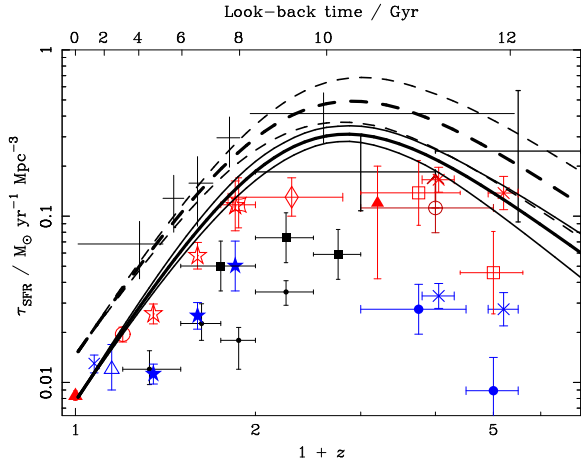


Figure 12. The history of star formation inferred using the methods discussed in §6.5. The thick solid line is derived using a simple parametric luminosity evolution model and the thick dashed line with a hierarchical model. Both have been revised since Blain et al. (1999b, 1999c) were published, to reflect the increased amount of far-IR and submm data now available. The thin lines show the envelope of 68-per-cent uncertainty for each of the two models. The relative vertical normalisation of the curves depends on the assumed IMF and the AGN fraction. The data points are inferred from UV/optical/near-IR observations, in order of increasing redshift, by Gallego et al. (1996; filled triangle), Gronwall (1999; thin diagonal cross), Treyer et al. (1998; open triangle), Tresse & Maddox (1998; empty circle), Lilly et al. (1996; filled stars), Cowie, Songaila & Barger (1999; small filled circles), Glazebrook et al. (1999; bent square at $z = 0.9$), Connolly et al. (1997; filled squares), Moorwood et al. (2000, filled triangle), Yan et al. (1999; empty lozenge), Madau et al. (1996; large filled circles), and Pettini et al. (1998; empty squares). Flores et al. (1999; empty stars) and Pettini et al. (1998) have corrected the Lilly et al. and Madau et al. results respectively for observed dust extinction. The high-redshift points are derived from analyses of the *HDF*. Wide-area ground-based surveys by Steidel et al. (1999) have increased the estimated high-redshift SFR, as shown by the thick diagonal crosses. No extinction correction is applied to these points; Steidel et al. (1999) estimate that the extinction-corrected SFR is greater by a factor of about 5; the effects are shown by the higher pair of diagonal crosses. At longer wavelengths, SFRs have been derived from mid-IR observations by Flores et al. (1999) and in the submm by Hughes et al. (1998; empty circle with upward pointing arrow). Based on radio observation, supplemented by redshift information provided by spectroscopic and photometric redshifts, Haarsma et al. (2000) infer star-formation rates shown by the thin solid crosses with no terminators. Based on a similar technique, supplemented further by submm observations, and including a completeness correction factor of 11, Barger, Cowie & Richards (2000) derive star-formation rates shown by the thick solid crosses with terminators.

6.5.2 A model of merging galaxies

Rather than use a purely parametric form for the evolution of $\Phi(L, z)$, an alternative approach is to adopt a more physically-motivated model based upon the merger of dark matter halos in the Press–Schechter formalism (Press & Schechter 1974). This implicitly assumes that the activity observed in the far-IR is triggered through interactions and mergers (see §6.1). We use a simple form of the evolution of the merger rate of dark-matter halos (Blain & Longair

1993; Blain et al. 1999c), which adequately reproduces the results of recent N -body simulations (Jenkins et al. 2001), and make the most basic assumption that a certain redshift-dependent fraction $x(z)$ of the total mass of dark and baryonic matter involved in these mergers is converted into energy by nucleosynthesis in high-mass stars with an efficiency $0.007c^2$. The same formalism is appropriate for describing the evolution of AGN fueling events at the epochs of mergers (Blain et al. 1999c). The form of evolution and normalization of $x(z)$ can be determined in the same manner as for the parametric model, using the background radiation intensity and low-redshift *IRAS* counts. Using an appropriate form of $x(z) = g(z)/(1+z)^{3/2}$ (Jameson 1999), we find best-fit parameters of $b = 1.95 \pm 0.1$, $c = 1.6 \pm 0.1$ and $x(0) = 1.35 \times 10^{-4}$ in our standard cosmology, assuming the same galaxy SED used in the parametric model. However, this model under-predicts the observed 175- and 850- μm counts by a large factor and so we are forced to introduce an additional parameter to allow the efficiency of merger-induced bursts of activity to increase at high redshifts so as to reproduce these long-wavelength source counts. This additional parameter is the product of the fraction F of mergers which generate luminous bursts and the duration of these bursts, σ . The product $F\sigma(z)$ is included in our model and then constrained using all the available far-IR counts, backgrounds and redshift distributions. Using the form $F\sigma(z) = F\sigma(0)\exp(az + bz^2 + cz^3)$, we derive values of $F\sigma(0) = 2.4 \text{ Gyr}$, $a = -4.14$, $b = -0.56$ and $c = 0.46$. The resulting history of galaxy evolution is shown by the thick dashed line in Fig. 12.

6.5.3 The star-formation history

Both the parametric and hierarchical models account for all the observed background radiation, counts and redshift distributions of galaxies at wavelengths longer than $60 \mu\text{m}$. As shown by the comparison of the models with the optical/UV derived data points in Fig. 12, the dominant source of energy in the Universe is the rest-frame far-IR radiation of starlight and AGN emission which has been reprocessed by dust. Indeed, apart from the relative normalisation (which can be varied by altering the assumed IMF and the fraction of AGN-powered activity), the parametric and hierarchical models in Fig. 12 show very similar behaviour. Equally the star-formation histories derived from deep radio selected samples also show a comparable behaviour (Cram 1998; Barger, Cowie & Richards 2000; Haarsma et al. 2000; Chapman et al. 2001), which also tend to lie above the optically-derived values, in broad agreement with the dust-enshrouded star-formation histories derived here (see Fig. 12). Note that the results of Barger et al. (2000) do not clearly indicate a decline in the high-redshift evolution of the star-formation rate.

In our hierarchical model, the strong increase in the far-IR luminosity density out to $z \sim 1-2$ arises in part from the increased rate of mergers in the early Universe. In addition, however, the ratio of the total amount of energy released during mergers and the mass of dark matter involved must increase sharply with redshift. This suggests that the progenitors of the submm galaxies which dominate the far-IR emission at high redshifts must be more prone to massive starbursts or AGN activity. This conclusion echoes the dis-

cussion of individual submm galaxies earlier in this section, where we find evidence that the typical separations between the components in these massive, gas-rich mergers maybe larger than has been claimed for similarly luminous galaxies locally. This also hints at an increased instability in the progenitor galaxies at high redshifts as the bolometric emission from massive, high-redshift mergers appears to peak earlier during their interaction. Finally, we note that to avoid biasing the redshift distribution of SCUBA-selected galaxies to very high redshifts (Blain et al. 1999b) and to remain consistent with the spectral index of the mm-wave extragalactic background radiation (Gispert, Lagache & Puget 2000), the comoving star-formation rate density in the obscured population must decline beyond $z \gtrsim 3$ –4.

The framework incorporated in our models can be extended to include (or predict) observations in the radio and mid-IR regimes. For example, assuming the standard form of the far-IR–radio correlation, with a radio spectral index of -0.65 , then the parametric and hierarchical models predict source surface densities brighter than $10 \mu\text{Jy}$ at 8.4 GHz of 1.05 and 0.98 arcmin^{-2} , with slopes of -1.4 and -1.3 respectively, closely matching the observed count $N(\geq S) = (1.01 \pm 0.14)(S/10\mu\text{Jy})^{-1.25 \pm 0.2}$ (Partridge et al. 1997). Whereas, adopting a simple form for the mid-IR region of our fiducial galaxy SED, $F_\nu \propto \nu^{+\alpha}$ with $\alpha = -1.95$ at $\lambda \lesssim 60 \mu\text{m}$, then we reproduce the normalization and general features of the deep $15\text{-}\mu\text{m}$ galaxy counts from *ISOCAM* (Elbaz et al. 1999), including the marked change of slope at flux densities between 0.5 and 1 mJy . The predicted slope of the $15\text{-}\mu\text{m}$ counts at flux densities between 1 and 10 mJy is steeper in the hierarchical model and provides slightly better agreement with the observations than the parametric scheme.

Finally, we note one outstanding problem with the star-formation histories derived from the far-IR, first highlighted by Blain et al. (1999b). This is that the predicted mass fraction in stars, Ω_* , at the present day, from these models, exceed the estimates of the observed stellar density by a factor of about five, based on a large near-IR-selected redshift survey by Cole et al. (2001). One possible explanation for this discrepancy is that a large fraction of the luminosity of distant dusty galaxies could be produced by AGN rather than by high-mass stars. However, the current estimates of the fraction of AGN-dominated submm sources presented in §6.4 suggest this is not likely (although this obviously requires confirmation, e.g. Ivison et al. 1998, 2000a; Almaini et al. 2001). This indicates, therefore, that if the background radiation intensity and counts determined in the submm waveband are not significantly in error then either a larger fraction of the baryons in the Universe has been processed into stars than is estimated from local galaxy surveys or, more likely, the process of star formation in the submm population must differ from that in nearby ‘normal’ galaxies, with an initial IMF biased to high-mass stars (more akin to the that seen in 30 Doradus, Sirianni et al. 2001). Blain et al. (1999b) estimated that a lower mass limit of about $1 M_\odot$ is required in the IMF in the submm galaxies to comply with the local stellar mass fraction, although higher mass cutoffs are also feasible.

7 DISCUSSION

There are several questions about the submm population which need to be urgently addressed. These concern the nature of the galaxies selected in the submm, their redshifts, masses and power sources, as well as more general issues of their relation to other classes of high-redshift sources, such as LBGs, radio galaxies and QSOs.

As this paper has demonstrated, we are still at a relatively early stage in our understanding of the mJy submm population. In part, this is because they were only discovered four years ago. However, as we have stressed here, the main barrier to improving our knowledge of this population is the lack of bright optical (or even near-IR) counterparts for the bulk of the submm galaxies found to date. As a result, we are left with relatively little evidence to sift when trying to understand the nature and evolution of this population and must fall back on circumstantial evidence and some degree of conjecture when attempting to place these galaxies within their correct cosmological context.

Integrating the deepest submm counts, we have shown that the submm galaxies lying in the decade of flux brighter than about 1 mJy produce about 60 per cent of the far-IR background at $850 \mu\text{m}$ (see also Hughes et al. 1998; Eales et al. 1999) and probably closer to 80 per cent by 0.5 mJy . Taken in combination with the fact that over half the energy density in the extragalactic background is contained in the far-IR and submm wavebands, it is clear that this population is important for understanding the energetics of galaxy formation and evolution.

The weight of evidence on the distances to these galaxies, from optical and near-IR spectroscopy and crude limits based on far-IR and radio colours, appears to point to the bulk of this population lying at high redshifts, $z > 2$. This confirms that for any reasonable characteristic dust temperature these dusty galaxies must have high bolometric luminosities, $\gtrsim 10^{12} L_\odot$, and thus classifies them as ULIRGs. The importance of this population at high redshifts is in stark contrast with its negligible contribution to their luminosity density at $z = 0$. Thus we must be seeing rapid evolution in these highly luminous systems.

On the question of what powers the immense luminosities of the submm population, again the balance of evidence is that majority of the population do not appear to host unobscured, or partially-obscured, AGN (e.g. Almaini et al. 2001), similar to the proportion of AGN-dominated ULIRGs seen locally (Genzel et al. 1998). Even in the few examples which do show clear signatures of non-thermal emission it appears that star formation still contributes a large fraction of the total bolometric output (Frayser et al. 1998; Bautz et al. 2000).

This then leaves us with massive star formation as the most likely mechanism to power these sources. The SFR required to produce $L_{\text{FIR}} \sim 10^{12} L_\odot$ corresponds to a formation rate of O, B and A stars of about $210 M_\odot \text{ yr}^{-1}$ (or an upper limit of $650 M_\odot \text{ yr}^{-1}$, based on an extrapolation using a Salpeter IMF extending from 0.1 to $100 M_\odot$, Thronson & Telesco 1986). These estimates are consistent with other measures of the SFR available for a handful of the submm population (Ivison et al. 2000a) and are sufficient to form an L^* -galaxy in only a few 100 Myr .

Next, we address the question of the relationship be-

tween the submm galaxies and other classes of high-redshift sources and the information these provide about galaxy formation as traced by the star-formation history of the Universe.

In a recent paper, Adelberger & Steidel (2000, AS) presented a useful analysis of the properties that submm galaxies would be expected assuming that they can be described by an extrapolation of the behaviour of the populations selected in the rest-frame UV. Based upon the rest-frame UV emission (observed R/I bands) and a model of the correlation between UV spectral slope and far-IR emission for local UV-detected starbursts, AS predict that the median magnitude of the counterparts to the 850- μm sources in our survey should be $I \sim 24$. However, as Table 4 shows, the lensing-corrected median apparent magnitude for our sample is actually $I \geq 26$, and may be considerably fainter as most of the sources remain undetected in I , even though some are seen in the K -band. This indicates that the UV/far-IR ratio of these submm-selected galaxies is roughly an order of magnitude lower than expected from AS's model.

Indeed, recent work by van der Werf et al. (2001a), Baker et al. (2001), Sanders (2001) and Meurer & Seibert (2001) has shown that the extrapolation used by AS is not followed by bolometrically-selected samples of very luminous local and distant galaxies. Hence, the basic assumption of AS's analysis – that the SFRs of luminous submm galaxies can be predicted reliably from their rest-frame UV emission – is unfounded (also see Chapman et al. 2000; Peacock et al. 2000). Moreover, given their extreme faintness in the optical, a large proportion of the submm galaxies are completely missed by UV-selected surveys of the distant Universe. Obviously any attempt to apply a correction factor for the star formation density missed in this population cannot rely on their (unmeasurable) UV spectral slopes. As a result, such surveys provide a lower limit to, but a potentially seriously incomplete measure of, the total star formation rate at high redshifts (Hughes et al. 1998).

If we assume instead that the bulk of the star formation traced by the submm population is completely missed in the UV, we must add their contribution to UV-based estimates to obtain the total star-formation density. Unfortunately, we still lack detailed information about the properties of the majority of submm galaxies (most crucially redshifts) and for this reason we therefore follow the approach of Blain et al. (1999b, 1999c) and use two simple evolutionary models to derive the history of star-formation activity using all available far-IR and submm background and count data. First, a model of pure-luminosity evolution of the low-redshift 60- μm *IRAS* luminosity function as described in detail by Blain et al. (1999b); second, a model of galaxy formation by hierarchical clustering, in which powerful episodes of dust-enshrouded luminosity are triggered by major mergers, as described by Blain et al. (1999c). The results of both models have been updated to include count and redshift data that was unavailable when these works were published, as described in §6.5, are shown in Fig. 12.

Subject to systematic uncertainties in the IMF (§6.5.3), and the fraction of energy released in dust-enshrouded galaxies due to AGN accretion as compared with high-mass star-formation activity, the total amount of star-formation in dust-enshrouded galaxies appears to exceed that within optical- and near-IR-selected galaxies at high redshift by a

factor of several (Fig. 12). Even after correcting the model results, assuming that at most 20 per cent of the emission comes from purely gravitationally-powered emission from AGN (§6.4; Almaini et al. 1999, 2001), the obscured activity in the far-IR selected galaxy population will still dominate the budget of massive star formation at $z \sim 2-3$ (Hughes et al. 1998). The properties of these galaxies are thus central to our understanding of the formation of massive stars and metals in the high-redshift Universe.

The classes of distant galaxies selected through submm and UV techniques clearly have very different properties and represent relatively independent subsets of the high-redshift galaxy population, except for rare composite systems such as SMM J14011+0252. What is the physical basis for these differences? Do the submm galaxies represent the most massive members of the galaxy population as a whole, or do they represent a particular evolutionary phase (Shu et al. 2001; Fardal et al. 2001; Granato et al. 2001)?

The dynamical information available for several Class-II submm galaxies shows them to be massive systems, $\gtrsim 10^{11} M_{\odot}$ within 20 kpc. This is nearly an order of magnitude more massive than typical UV-selected galaxies at $z > 2$ which have a comparable volume density (Pettini et al. 1998; Moorwood et al. 2000; Kobulnicky & Koo 2001), although a small proportion of equally massive LBGs are known (e.g. Pettini et al. 1998, 2001). The rest-frame optical sizes of the Class-II submm galaxies also appear to be larger than is typically found for UV-selected sources (compare the results in Ivison et al. 2000a and Dickinson 2000) with several showing merger-like morphologies.

Thus, while there is some evidence to suggest that the submm galaxies have more massive progenitors than the typical LBGs (see also Shu et al. 2001), we are more inclined to believe that they represent a particular phase in the evolution of massive galaxies at high redshifts, rather than a completely separate population.

The Class-II submm galaxies are optically luminous and yet gas-rich, indicating that they possess both a significant mass of existing stars, and a substantial reservoir of fuel for the formation of additional stellar populations. This suggests that the present-day descendants of these galaxies will be some of the most massive stellar systems in the local Universe. It is the properties of these Class-II galaxies which are at the heart of the argument that submm galaxies evolve into the most luminous and massive spheroids ($\gtrsim L^*$) at the present day. The merger-like morphologies of some of these galaxies is further evidence for their role in forming the most massive local ellipticals. Support for this argument for the general submm population is entirely circumstantial: their strong clustering (Ivison et al. 2000b; Almaini et al. 2001) and equivalent space density to local luminous ellipticals (Lilly et al. 1999). However, to construct a more direct evolutionary connection will require kinematically-selected samples of high-redshift galaxies, and as such will be observationally demanding.

Further depletion of the gas reservoir in the Class-II galaxies and the destruction of obscuring dust by intense radiation fields would naturally result in them evolving into massive examples of LBGs, QSO host galaxies or luminous radio galaxies (Dunlop 2001; Granato et al. 2001). If the Class-II sources represent the most evolved submm galaxies, then the pressing question is the relationship between

these and the majority of the submm population, which fall into Class 0/I. Do these optically-fainter systems represent either higher redshift systems, or an earlier phase in the growth of the Class-II galaxies, i.e. does the Class 0–II classification scheme have an evolutionary basis akin to that for protostars, or are Class 0/I galaxies simply their less massive cousins, or intrinsically more obscured?

Our sample shows slight differences between Class-0/I and Class-II sources, with the suggestion that the former are typically fainter in the submm and exhibit higher radio–submm indices, $\alpha_{1.4}^{850}$. The simplest interpretations are that the Class-0/I sources include some galaxies that either are more obscured, or have intrinsically colder dust, or lie at higher redshifts than the Class-II sources. We note that the median redshift of the Class-II galaxies is $\langle z \rangle = 1.9 \pm 0.6$, compared to the estimate of $\langle z \rangle = 2.8_{-1.2}^{+2.1}$ from the radio–submm index-based estimates for the Class-0/I sources. This hints that at least some of the Class-0/I galaxies may be at high redshifts, $z \gtrsim 3$, where K -corrections would dim their near-IR counterparts significantly (Fig. 8; Dey et al. 1999). However, the current sample is too small and the uncertainties too large to clearly show any differences between the classes or definitively state the reasons for these.

8 CONCLUSIONS

In summary, the bulk of the background radiation intensity has been resolved into discrete submm sources using SCUBA at an 850- μm intrinsic flux limit of ~ 1 mJy. The counterparts to these submm sources appear to be dusty, ultraluminous galaxies with very diverse optical and near-IR properties. The majority of these galaxies appear to lie at $z \gtrsim 1$, with a median redshift of $z \sim 2.5$ –3.

The optically brighter sources have been studied in more detail using mm-wave interferometers, and they show the large dynamical masses and high gas fractions expected for young massive galaxies. The characteristics of these galaxies are consistent with them being the progenitors of the most massive elliptical galaxies seen in the local Universe. A comparison of the detailed properties of a handful of these galaxies with local ULIRGs suggests that the rapid increase in dust-obscured activity at high redshifts, need to explain the submm counts and the FIRB, has its origin in the increasing instability of the gas-rich, bulge-weak progenitors of the submm population at high redshifts. However, the majority of the mJy submm population remain elusive; they have very faint (or invisible) counterparts in the optical and near-IR and progress in investigating their nature and properties is likely to be slow.

In the future we look forward to increases in the number of submm galaxies with accurate redshift determinations – crucial for follow-up CO line-mapping to provide dynamical masses and gas fractions. Work in this area will require deep spectroscopy in the near-IR (and optical) on 10-m class telescopes for the brighter Class-I and II sources, as well as more innovative approaches, such as blind radio searches for OH/H₂O maser emission (Townsend et al. 2001). Improved constraints on the redshift distribution of the whole submm population await the confirmation of the radio-submm spectral index (and more detailed SED fitting) as a reliable estimator of redshift for submm-selected galaxies. In part this

will rely on checking at higher luminosities and redshifts, using *SIRTf* and *SOFIA*, the relatively weak dependence of dust temperature on luminosity seen in low-redshift *IRAS*-selected galaxies by Dunne et al. (2000).

Equally essential is the detailed study of the characteristics of individual sources. Here the main advances are likely to come from observations across a wide range of wavelength, with the X-ray, mid-IR and far-IR wavebands being the most promising, providing crucial information about the distribution of dust temperatures and the power sources driving these systems. Observations at higher spatial resolution, in the near-IR, mm and radio wavebands, will allow us to study the internal structure of these galaxies – to search for morphological evidence of the events which triggered their prodigious activity. In particular, the refurbishment of *NICMOS* on-board *HST* will provide a powerful tool to interpret the rest-frame optical morphologies of these galaxies and compare them to local ULIRGs to test if the same physical processes are responsible for ultraluminous systems at low and high redshifts. In the longer term, the direct study of the detailed astrophysics of submm galaxies will benefit immensely from the sensitivity and resolving power of the 10-milliarcsec resolution ALMA interferometer array.

We expect that submm surveys which exploit lens amplification, such as the one presented here, will retain a central role in studying the submm galaxy population. In part this is because the properties of these galaxies tax the capabilities of current instrumentation in many wavebands and hence the boost provided by the lens is essential for successful follow-up. Moreover, observations through massive gravitational lenses allow us to probe intrinsically fainter submm sources, which are more representative of the population responsible for the bulk of the FIRB. We look forward to continued exploitation of the sample presented here, and the results of new surveys, to study the nature of the faint submm population and answer some of the questions raised in this paper.

Finally, the goal of future theoretical work in this area should be to incorporate both the obscured submm population (Class 0 and I) and the less-obscured systems (Class-II submm galaxies and the more massive classical LBGs) into a single evolutionary sequence and hence naturally explain the relation between the two populations. Important observational input on this question can be obtained by studying the relative clustering of the various populations in well-defined environments at high redshifts, in particular the overdense regions around some luminous radio galaxies (Ivison et al. 2000b) may evolve into the cores of massive clusters at the present day. Such studies will require wide-field surveys covering the UV, near-IR and longer wavelengths, the new SCUBA2 submm camera for the JCMT and the WFCAM panoramic near-IR camera for UKIRT will be a powerful facilities for obtaining the essential observations in these wavebands.

ACKNOWLEDGEMENTS

We would like to thank Amy Barger, Len Cowie, Alastair Edge, Dave Frayer, Katherine Gunn, Frazer Owen and Ian Robson for help in undertaking this project. We also thank Bruno Altieri, Carlton Baugh, Chris Carilli, Scott Chap-

man, Shaun Cole, Danny Dale, James Dunlop, Harald Ebeling, Steve Eales, Richard Ellis, Andy Fabian, Carlos Frenk, Allon Jameson, Cedric Lacey, Andy Lawrence, Simon Lilly, Malcolm Longair, Leo Metcalfe, Chris Mihos, Glenn Morrison, Matt Page, Max Pettini, Bianca Poggianti, Michael Rowan-Robinson, Nick Scoville, Jason Stevens, Neil Trentham, Paul van der Werf and Min Yun for useful conversations and help. Finally, we acknowledge the first anonymous referee for her comments and thank the second referee for their thorough reading of this manuscript and suggestions for improvements. IRS acknowledges support from the Royal Society and the Leverhulme Trust, RJI from PPARC, AWB thanks the Raymond and Beverly Sackler Foundations and JPK the CNRS.

REFERENCES

- Adams F.C., Lada C.J., Shu F.H., 1987, *ApJ*, 312, 788
 Adelberger K.L., Steidel C.C., 2000, *ApJ*, 544, 218 [AS]
 Almaini O., Lawrence A., Boyle B.J., 1999, *MNRAS*, 305, L59
 Almaini O., Scott S.E., Dunlop J.S., Manners J.C., Willott C.J., Lawrence A., et al., 2001, submitted
 Altieri B., Metcalfe L., Kneib J.-P., McBreen B., Aussel H., Biviano A., et al., 1999, *A&A*, 343, 65
 Baker A.J., Lutz D., Genzel R., Tacconi L.J., Lehnert M.D., 2001, *A&A*, 372, 37
 Barger A.J., Cowie L.L., Sanders D.B., Fulton E., Taniguchi Y., Sato Y., Kawara K., Okuda H. 1998, *Nature*, 394, 248
 Barger A.J., Cowie L.L., Smail I., Ivison R.J., Blain A.W., Kneib J.-P., 1999a, *AJ*, 117, 2656
 Barger A.J., Cowie L.L., Sanders D.B., 1999b, *ApJ*, 518, L5
 Barger A.J., Cowie L.L., Richards E.A., 2000, *AJ*, 119, 2092
 Barnard V.E., Blain A.W., 2001, *MNRAS*, submitted
 Baugh C.M., Cole S., Frenk C.S., Lacey C.G., 1998, *ApJ*, 498, 504
 Bautz M.W., Malm M.R., Baganoff F.K., Ricker G.R., Canizares C.R., Brandt W.N., Hornschemeier A.E., Garmire G.P., 2000, *ApJ*, 543, L119
 Bekki K., Shioya Y., Tanaka I., 1999, *ApJ*, 520, L99
 Benford D.J., Cox P., Omont A., Phillips T.G., McMahon R.G., 1999, *ApJ*, 518, 65
 Bernstein R.A., Freedman W., Madore B., 2001, *ApJ*, submitted
 Bertin E., Arnouts S., 1996, *A&A*, 117, 393
 Bertoldi F., Carilli C.L., Menten K.M., Owen F., Dey A., Gueth F., et al., 2000, *A&A*, 360, 92
 Biviano A., Metcalfe L., Altieri B., Leech K., Schulz B., McBreen B., Delaney M., 2000, in *Clustering at High Redshifts*, eds. Mazure, A., Le Fèvre, O., Le Brun, V., *Astron. Soc. Pac.*, San Francisco, p. 101 (astro-ph/9910314)
 Blain A.W., 1998, *MNRAS*, 290, 553
 Blain A.W., 1999, *MNRAS*, 309, 955
 Blain A.W., 2001, in *Starbursts near and far*, ed. Lutz D., Tacconi L., Springer, in press (astro-ph/0011387)
 Blain A.W., Longair M.S., 1993, *MNRAS*, 265, L21
 Blain A.W., Ivison R.J., Smail I., 1998, *MNRAS*, 296, L29
 Blain A.W., Kneib J.-P., Ivison R.J., Smail I., 1999a, *ApJ*, 512, L87
 Blain A.W., Smail I., Ivison R.J., Kneib J.-P., 1999b, *MNRAS*, 302, 632
 Blain A.W., Jameson, A., Smail I., Longair, M.S., Kneib J.-P., Ivison R.J., 1999c, *MNRAS*, 309, 715
 Blain A.W., Ivison R.J., Kneib J.-P., Smail I., 2000, in *The High-Redshift Universe*, eds. Bunker A.J., van Breugel W.J.M., ASP, San Francisco, p. 246 (astro-ph/9906024)
 Borys C., Chapman S., Halpern M., Scott D., 2001, in *UMass/INAOE Conference on Deep Millimeter Surveys*, eds. Lowenthal J., Hughes D.
 Carilli C.L., Yun M.S., 1999, *ApJ*, 513, L13
 Carilli C.L., Yun M.S., 2000, *ApJ*, 530, 618
 Casali M.M., Hawarden T., 1992, *UKIRT-JCMT Newsletter*, 3, 33
 Chapman S.C., Scott D., Steidel C.C., Borys C., Halpern M., Morris S.L., et al., 2000, *MNRAS*, 319, 318
 Chapman S.C., Scott D., Borys C., Fahlman G.G., 2001a, *MNRAS*, submitted (astro-ph/0009067)
 Chapman S.C., Richards E.A., Lewis G., Wilson G., Barger A., 2001b, *ApJ*, 548, L147
 Chapman S.C., Lewis G.F., Scott D., Borys C., Richards E.A., 2001c, *ApJ*, in press
 Chapman S.C., Smail I., Ivison R.J., Helou G., Dale D., Lagache G., 2002, *ApJ*, submitted
 Cole S., Norberg P., Baugh C.M., Frenk C.S., et al., 2001, *MNRAS*, 326, 255
 Condon J.J., 1992, *ARAA*, 30, 575
 Connolly A.J., Szalay A.S., Dickinson M., Subbarao M.U., Brunner R.J., 1997, *ApJ*, 486, L11
 Cowie L.L., Songaila, A., Barger A.J., 1999, *AJ*, 118, 603
 Cram L., 1998, *ApJ*, 506, L85
 Dale D.A., Helou G., Contursi A., Silbermann N.A., Kolhatkar S., 2001, *ApJ*, 549, 215
 Dey A., Graham J.R., Ivison R.J., Smail I., Wright G.S., Liu M., 1999, *ApJ*, 519, 610
 Dickinson M.E., 2000, *Phil. Tran. Roy. Soc.*, in press (astro-ph/0004028)
 Downes D. Solomon, P.M., 1998, *ApJ*, 509, 615
 Downes D., Neri R., Greve A., Guilloteau S., Casoli F., Hughes D., Lutz D., et al., 1999, *A&A*, 347, 809
 Dunlop J.S., 2001, in *UMass/INAOE Conference on Deep Millimeter Surveys*, eds. Lowenthal J., Hughes D., in press (astro-ph/0011007)
 Dunne L., Clements D.L., Eales S.A., 2000, *MNRAS*, 319, 813
 Dunne L., Eales S.A., Edmunds M.G., Ivison R.J., Alexander P., Clements, D., 2000, *MNRAS*, 315, 115
 Dunne L., Eales S.A., 2001, *MNRAS*, 327, 697
 Eales S.A., Lilly S.J., Gear W.K., Dunne L., Bond J.R., Hammer F., Le Fèvre O., Crampton D., 1999, *ApJ*, 515, 518
 Eales S., Lilly S., Webb T., Dunne L., Gear W., Clements D., Yun M., 2000, *AJ*, 120, 2244
 Edge A.C., Ivison R.J., Smail I., Blain A.W., Kneib J.-P., 1999, *MNRAS*, 306, 599
 Elbaz D., Cesarsky C.J., Fadda D., Aussel H., Desert F.X., Franceschini A., et al., 1999, *A&A*, 351, L37
 Fabian A.C., Smail I., Iwasawa K., Allen S.W., Blain A.W., Crawford C.S., Ettori S., Ivison R.J., Johnstone R.M., Kneib J.-P., Wilman R.J., 2000, *MNRAS*, 315, L8
 Fardal M.A., Katz N., Weinberg D.H., Davee R., Hernquist, L., 2001, *ApJ*, submitted
 Finkbeiner D.P., Schlegel D.J., Davis M., 2000, *ApJ*, 524, 867
 Fixsen D.J., Dwek E., Mather J.C., Bennett C.L., Shafer R.A., 1998, *ApJ*, 508, 123
 Flores H., Hammer F., Thuan T.X., Césarsky C., Desert F.X., Omont A., et al., 1999, *ApJ*, 517, 148
 Fox M.J., Efstathiou A., Rowan-Robinson M., Dunlop J.S., Scott S., Serjeant S., et al., 2001, *MNRAS*, submitted
 Frayer D.T., Ivison R.J., Scoville N.Z., Evans A.S., Yun M., Smail I., Blain A.W., Kneib J.-P., 1998, *ApJ*, 506, L7
 Frayer D.T., Ivison R.J., Scoville N.Z., Evans A.S., Yun M., Smail I., Barger A.J., Blain A.W., Kneib J.-P., 1999, *ApJ*, 514, L13
 Frayer D.T., Smail I., Ivison R.J., Scoville N.Z., 2000, *AJ*, 120, 1668
 Gallego J., Zamorano J., Aragón-Salamanca A., Rego M., 1996, *ApJ*, 459, L43
 Gear W.K., Lilly S.J., Stevens J.A., Clements D.L., Webb T.M.,

- Eales S.A., Dunne L., 2000, MNRAS, 316, L51
- Gehrels N., 1986, ApJ, 303, 336
- Genzel R., Lutz D., Sturm E., Egami E., Kunze D., et al., 1998, ApJ, 498, 579
- Glazebrook K., Blake C., Economou F., Lilly S., Colless M., 1999, MNRAS, 306, 843
- Granato, G.L., Silva, L., Monaco, P., Panuzzo, P., Salucci, P., De Zotti, G., Danese, L., 2001, MNRAS, submitted
- Gronwall C., 1999, in After the dark ages: when galaxies were young, eds. Holt S., Smith E., AIP, Woodbury, NY, p. 335
- Gispert R., Lagache G., Puget J.-L., 2000, A&A, 360, 1
- Guiderdoni B., Hivon E., Bouchet F.R., Maffei B., 1998, MNRAS, 295, 877
- Gunn K.F., Shanks T., 2001, MNRAS, submitted (astro-ph/9909089)
- Haarsma D.B., Partridge R.B., Windhorst R.A., Richards E.A., 2000, ApJ, 544, 641
- Ho P.T.P., 2000, in Imaging at radio through submillimeter wavelengths, ed. J. Mangum, ASP Conf. Ser. vol. 217, p. 227
- Hogg D.W., 2001, AJ, 121, 1207
- Holland W.S., Robson E.I., Gear W.K., Cunningham C.R., Lightfoot J.F., Jenness T., et al., 1999, MNRAS, 303, 659
- Hornschemeier A.E., Brandt W.N., Barmire G.P., Schneider D.P., Broos P.S., Townsley L.K., et al., 2000, ApJ, 541, 49
- Hughes D.H., Serjeant S., Dunlop, J., Rowan-Robinson, M., Blain A., Mann R.G., et al., 1998, Nature, 394, 241
- Ivison R.J., Dunlop J.S., Hughes D.H., Archibald E.N., Stevens J.A., et al., 1998b, ApJ, 494, 211
- Ivison R.J., Smail I., Le Borgne J.-F., Blain A.W., Kneib J.-P., Bézecourt J., Kerr T.H., Davies J.K., 1998a, MNRAS, 298, 583
- Ivison R.J., Smail I., Blain A.W., Kneib J.-P., Frayer D.T., 1999, Ap&SS, 266, 285
- Ivison R.J., Smail I., Barger A., Kneib J.-P., Blain A.W., Owen F.N., Kerr T.H., Cowie L.L., 2000a, MNRAS, 315, 209
- Ivison R.J., Dunlop J.S., Smail I., Dey A., Graham J.R., Liu M.C., 2000b, ApJ, 542, 271
- Ivison R.J., Smail I., Dunlop J.S., Jenner C.J., 2001a, in UMass/INAOE Conference on Deep Millimeter Surveys, eds. Lowenthal J., Hughes D., in press
- Ivison, R.J., Smail, I., Frayer, D.T., Kneib, J.-P., Blain, A.W., 2001b, ApJL, 561 L45
- Jameson A., 1999, PhD thesis, University of Cambridge
- Jenness T., 1997, Starlink User Note 216.1
- Jenkins A., Frenk C.S., White S.D.M., Colberg J.M., Cole S., Evrard A., Couchman H.M.P., Yoshida N., 2001, MNRAS, 321, 372
- Juvela M., Mattila K., Lemke D., 2000, A&A, 360, 813
- Kaspi S., Brandt W.N., Schneider D.P., 2000 AJ, 119, 2031
- Kneib J.-P., Ellis R.S., Smail I., Couch W.J., Sharples R.M., 1996, ApJ, 471, 643
- Kneib J.-P., Prieur J.-L., Ivison R.J., Smail I., Blain A.W., 2002, A&A, in prep
- Kobulnicky H.A., Koo D.C., 2001, ApJ, 545, 712
- Lémonon L., Pierre M., Cesarsky C.J., Elbaz D., Pelló R., Soucaïl G., Vigroux L., 1998, A&A, 334, L21
- Lilly S.J., Le Fèvre O., Hammer F., Crampton D., 1996, ApJ, 460, L1
- Lilly S.J., Eales S.A., Gear W.K.P., Hammer F., Le Fèvre O., Crampton D., Bond J.R., Dunne L., 1999, ApJ, 518, 641
- Lisenfeld U., Isaak K.G., Hills R., 2000, MNRAS, 312, 433
- Lutz D., Dunlop J.S., Almaini O., Andreani P., Blain A.W., Efstathiou A., 2001, A&A, 378, L70
- Madau P., Ferguson H.C., Dickinson M.E., Giavalisco M., Steidel C.C., Fruchter A., 1996, MNRAS, 283, 1388
- McMahon R.G., Priddey R.S., Omont A., Snellen I., Withington S., 1999, MNRAS, 309, L1
- Metcalfe L., Altieri B., McBreen B., Kneib J.-P., Delaney M., et al., 1999, in The Universe as seen by ISO, eds. Cox P., Kessler M.F., ESA Publication Division, ESTEC, Noordwijk, NL
- Meurer G.R., Seibert M., 2001, in Starbursts near and far, ed. Lutz D., Tacconi L., Springer, in press (astro-ph/0101479)
- Mihos J.C., Hernquist L., 1996, ApJ, 464, 641
- Moorwood A.F.M., van der Werf P., Cuby J.G., Oliva E., 2000, A&A, 362, 9
- Morrison G.E., 1999, PhD Thesis, University of New Mexico
- Murphy T.W., Armus L., Matthews K., Soifer B.T., Mazzarella J.M., Shupe D.L., Strauss M.A., Neugebauer G., 1996, AJ, 111, 1025
- Omont A., Petitjean P., Guilloteau S., McMahon R.G., Solomon P.M., Pecontal E., 1996, Nature, 382, 428
- Page M.J., et al., 2001, Science, in press
- Papadopoulos P., Ivison R.J., Carilli C., Lewis G., 2001, Nature, 409, 58
- Partridge R.B., Richard E.A., Fomalont E.B., Kellermann K.I., Windhorst R.A., 1997, ApJ, 483, 38
- Peacock J.A., Rowan-Robinson M., Blain A.W., Dunlop J.S., Efstathiou A., Hughes D.H., et al., 2000, MNRAS, 318, 535
- Pettini M., Kellogg M., Steidel C.C., Dickinson M., Adelberger K., Giavalisco M., 1998, ApJ, 508, 539
- Pettini M., Shapley A.E., Steidel C.C., Cuby J.-P., Dickinson M., Moorwood A.F.M., Adelberger K., Giavalisco M., 2001, ApJ, 554
- Pozzetti L., Mannucci F., 2000, MNRAS, 317, L17
- Press W.H., Schechter P., 1974, ApJ, 187, 425
- Puget J.-L., Abergel A., Bernard J.-P., Boulanger, F., Burton W.B., Desert F.-X., Hartmann D., 1996, A&A, 308, L5
- Puget J.-L., Lagache G., Clements D.L., Reach W.T., Aussel H., Bouchet F.R., et al., 1999, A&A, 345, 29
- Reach W.T. et al., 1995, ApJ, 451, 188
- Rigopoulou D., Spoon H.W.W., Genzel R., Lutz D., Moorwood A.F.M., Tran Q.D., 1999, AJ, 118, 2625
- Richards E.A., 1999, ApJ, 513, L9
- Rowan-Robinson M., 2001, ApJ, 549, 745
- Salasnich B., Girardi L., Weiss A., Chiosi C., 2000, A&A, 361, 1023
- Sanders D.B., Mirabel I.F., 1996, ARA&A, 34, 749
- Sanders D.B., Soifer B.T., Elias J.H., Madore B.F., Matthews K., Neugebauer G., Scoville N.Z., 1988, ApJ, 325, 74
- Sanders D.B., 2001, in UMass/INAOE Conference on Deep Millimeter Surveys, eds. Lowenthal J., Hughes D., in press
- Saunders W., Rowan-Robinson M., Lawrence A., Efstathiou G., Kaiser N., Ellis R.S., Frenk C.S., 1990, MNRAS, 242, 318
- Scott S., Fox M., Dunlop J.S., Serjeant S., Peacock J.A., Ivison R.J., et al., 2001, MNRAS, submitted
- Shu C., Mao S., Mo H.J., 2001, MNRAS, 327, 895
- Sirianni M., Nota A., Leitherer C., de Marchi G.D., Clampin M., ApJ, 2000, 533, 203
- Smail I., Ivison R.J., Blain A.W., 1997, ApJ, 490, L5
- Smail I., Ivison R.J., Blain A.W., Kneib J.-P., 1998, ApJ, 507, L21
- Smail I., Ivison R.J., Kneib J.-P., Cowie L.L., Blain A.W., Barger A.J., Owen F.N., Morrison G., 1999a, MNRAS, 308, 1061
- Smail I., Morrison G., Gray, M.E., Owen F.N., Ivison R.J., Kneib J.-P., Ellis R.S., 1999b, ApJ, 525, 609
- Smail I., Ivison R.J., Owen F.N., Blain A.W., Kneib J.-P., 2000, ApJ, 528, 612
- Smith G.P., Kneib J.-P., Ebeling H., Czoske O., Smail I., 2001a, ApJ, 552, 493
- Smith, G.P., Smail, I., Kneib, J.-P., Czoske, O., Ebeling, H., Edge, A.C., Pelló, R., Ivison, R.J., Packham, C., Le Borgne, J.-F., 2001b, MNRAS, in press.
- Soifer B.T., Neugebauer G., Houck J.R., 1987, ARA&A, 25, 187
- Soifer B.T., Neugebauer G., 1990, AJ, 101, 354
- Solomon P.M., 2001, in Starbursts near and far, ed. Lutz D.,

- Tacconi L., Springer, in press (astro-ph/0101482)
- Solomon P.M., Downes D., Radford S.J.E., Barrett J.W., 1997, *ApJ*, 478, 144
- Soucail G., Kneib J.-P., Bézecourt J., Metcalfe L., Altieri B., Le Borgne J.-F., 1999, *A&A*, 343, L70
- Steidel C.C., Adelberger K.L., Dickinson M., Giavalisco M., Pettini M., 1999, *ApJ*, 519, 1
- Thronson H.A., Telesco C.M., 1986, *ApJ*, 311, 98
- Townsend R.H.D., Ivison R.J., Smail I., Blain A.W., Frayer D.T., 2001, *MNRAS*, 328, L17
- Trentham N., Kormendy J., Sanders D., 1999, *AJ*, 117, 1152
- Tresse L., Maddox S.J., 1998, *ApJ*, 495, 691
- Treyer M. A., Ellis R.S., Milliard B., Donas J., Bridges T.J., 1998, *MNRAS*, 300, 303
- van der Werf P.P., Knudsen K.K., Labbé I., Franx M., 2001a, in *UMass/INAOE Conference on Deep Millimeter Surveys*, eds. Lowenthal J., Hughes D., in press (astro-ph/0011217)
- van der Werf P.P., et al., 2001b, in prep
- Vernet J., Cimatti A., 2001, *A&A*, in press
- Xu C., 2000, *ApJ*, 541, 134
- Yan L., McCarthy P.J., Freudling W., Teplitz H.I., Malumuth E.M., Weymann R.J., Malkan M.A., 1999, *ApJ*, 519, L47

Table 4. Photometry and limits (2σ)

Source	S_{850} (mJy)	T_{UKIRT} (ks)	K	$(R - K)$	$(I - K)$	Amp.	Comments
SMM J02399-0136	23.0	4.3	17.8±0.1	3.4±0.1	2.7±0.1	2.5	L1/L2 ^a
SMM J00266+1708	18.6	3.2	22.5±0.1 ^b	...	> 3.7	2.4	M12 ^b
SMM J09429+4658	17.2	8.1	19.4±0.3	> 4.4	> 6.0	2.0	H5 ^c
SMM J14009+0252	14.5	9.2	21.0±0.4	> 5.6	> 2.2	1.5	J5 ^d , R limit from new <i>WFPC2</i> data
SMM J14011+0252	12.3	7.0	17.6±0.1	3.7±0.1	3.1±0.1	2.8	J1/J2 ^d
SMM J02399-0134	11.0	9.2	16.3±0.2	4.3±0.2	3.0±0.3	2.5	L3 ^e
SMM J22471-0206	9.2	19.3	17.5±0.1	...	4.0±0.1	1.9	P4?
SMM J02400-0134	7.6	9.2	> 21.6	> 1.9	Blank ^f , $I > 26$
SMM J04431+0210	7.2	3.2	19.1±0.1	> 6.7	> 6.7	4.4	N4 ^c
SMM J21536+1742	6.7	10.4	> 21.6	...	< 3.8	1.9	K2? $I \sim 25.4$
SMM J00265+1710	6.1	4.8	> 21.0	> 2.3	Blank?, $I > 25$
SMM J22472-0206	6.1	7.6	> 21.4	...	< 2.4	2.2	P2? $I = 23.8$
SMM J00266+1710	5.9	3.2	> 20.9	> 3.6	Blank?, $I > 26$
SMM J00267+1709	5.0	3.2	> 20.7	> 2.2	Blank ^f , $I \gtrsim 25.5$
SMM J04433+0210	4.5	3.2	> 20.8	...	< 3.4	1.5	N5 $I = 24.2$
Cluster Galaxies							
SMM J21536+1741	9.1	10.4	13.2±0.0	...	2.5±0.0	...	A 2390 cD ^g
SMM J14010+0252	5.4	7.0	12.4±0.0	...	3.0±0.0	...	A 1835 cD ^g

a) Ivison et al. (1998a) – b) Frayer et al. (2000) – c) Smail et al. (1999a) – d) Ivison et al. (2000a) – e) Soucaill et al. (1999) – f) Smail et al. (1998) – g) Edge et al. (1999).

Table 5. Spectroscopy and redshift constraints

Source	S_{850} (mJy)	$S_{1.4}$ (μJy)	$\alpha_{1.4}^{850}$	z_{α}	z_{spec}^e		z_{SED}	Comments
					Reliable	Possible		
SMM J02399-0136	23.0	526	0.70 ± 0.02	0.9–2.3	2.80	L1/L2 – Sy 2 merger ^a
SMM J00266+1708	18.6	100	0.95 ± 0.04	2.0–5.0	2–5	M12 – ERO? ^b
SMM J09429+4658	17.2	32	1.14 ± 0.07	>3.4	2–4	H5 – ERO ^c
SMM J14009+0252	14.5	529	0.60 ± 0.03	0.7–1.8	3–5	J5 ^c – ERO ^d
SMM J14011+0252	12.3	115	0.85 ± 0.05	1.5–3.6	2.56	J1/J2 – starburst merger ^d
SMM J02399-0134	11.0	~500	0.55 ± 0.04	0.6–1.5	1.06	L3 – Sy 1.5/2 ring galaxy ^f
SMM J22471-0206	9.2	<65	> 0.90 ± 0.08	>1.7	...	1.16	...	P4? – weak AGN?
SMM J02400-0134	7.6	<33	> 0.99 ± 0.11	>2.2	Blank field ^g
SMM J04431+0210	7.2	<70	> 0.84 ± 0.10	>1.4	2–4	N4 – ERO ^c
SMM J21536+1742	6.7	1.60?	...	K2?
SMM J00265+1710	6.1	≤110	≥ 0.73 ± 0.07	>1.0	Blank field?
SMM J22472-0206	6.1	<50	> 0.87 ± 0.12	>1.6	...	2.11?	...	P2?
SMM J00266+1710	5.9	<33	> 0.93 ± 0.12	>1.9	Blank field?
SMM J00267+1709	5.0	<30	> 0.92 ± 0.13	>1.8	Blank field ^g
SMM J04433+0210	4.5	70	0.75 ± 0.12	1.1–2.7	N5
Cluster Galaxies								
SMM J21536+1741	9.1	226 × 10 ³	−0.58 ± 0.05	...	0.23	A 2390 cD ^h
SMM J14010+0252	5.4	28.6 × 10 ³	−0.30 ± 0.06	...	0.25	A 1835 cD ^h

a) Ivison et al. (1998a) – b) Frayer et al. (2000) – c) Smail et al. (1999a) – d) Ivison et al. (2000a) – e) Barger et al. (1999a) – f) Soucaill et al. (1999) – g) Smail et al. (1998) – h) Edge et al. (1999).